AJRCMB Articles in Press. Published on 27-February-2019 as 10.1165/rcmb.2018-0352OC

Phosphorylation of GMFγ by c-Abl coordinates lamellipodial and focal adhesion dynamics to regulate airway smooth muscle cell migration

Brennan D. Gerlach[1], Kate Tubbesing[1], Guoning Liao[1], Alyssa C. Rezey[1], Ruping Wang[1], Margarida Barroso[1] and Dale D. Tang[1]*

[1]Department of Molecular Cellular Physiology, Albany Medical College, Albany, New York, U.S.A. *Correspondence addressed to D.D.T. (tangd@amc.edu)

AUTHOR CONTRIBUTIONS

B.D.G performed and analyzed the majority of experiments. B.D.G, G.L, A.R, and R.P. generated DNA constructs and shRNA knockdown cells. B.D.G., K.T., and M.B. performed imaging and Imaris analysis. B.D.G. wrote manuscript. B.D.G., K.T., M.B., and D.D.T. reviewed and edited manuscript. D.D.T. supervised the study.

COMPETING FINANCIAL INTERESTS

The authors declare no competing financial interests.

Abstract

Airway smooth muscle cells require coordinated protrusion and focal adhesion dynamics to migrate properly. However, the signaling cascades that connect these two processes remain incompletely understood. GMFγ has been implicated in inducing actin debranching and inhibiting nucleation. In this study, we discovered that GMFγ phosphorylation at Y104 regulates human airway smooth muscle cell migration. Utilizing high-resolution microscopy coupled with 3D-object based quantitative image analysis software Imaris 9.2.0, phosphomimetic mutant Y104D-GMFγ was enriched at nascent adhesions along the leading edge where it recruited activated N-WASP (pY256) to promote actin-branch formation, which enhanced lamellipodial dynamics and limited the growth of focal adhesions. Unexpectedly, we found that non-phosphorylated mutant Y104F-GMFγ was enriched in growing adhesions where it promoted a linear branch organization, focal adhesion clustering, and recruited zyxin to increase maturation, thus inhibiting lamellipodial dynamics and cell migration. The localization of GMFγ between the leading edge and focal adhesions was dependent upon myosin activity. Furthermore, c-Abl tyrosine kinase regulated the GMFγ phosphorylation-dependent processes. Together, these results unveil the importance of GMFγ phosphorylation in coordinating lamellipodial and focal adhesion dynamics to regulate cell migration.

Introduction

Smooth muscle cell migration is critical for the development of airways, vasculature, gut, and bladder; however, it also contributes to the progression of diseases such as asthma (1-4). Cell migration involves the extension of membrane protrusions (lamellipodia and filopodia) and attachment of adhesive structures (focal adhesions) to the extracellular matrix, which together, generate mechanical tension to propel the cell through its environment (5, 6). The formation of the lamellipodia is established through dynamic actin

AJRCMB Articles in Press. Published on 27-February-2019 as 10.1165/rcmb.2018-0352OC

network assembly that is regulated by the Actin related protein 2/3 (Arp2/3) complex (1, 7-9). Nucleation promoting factors (NPFs) such as Neural Wiskott-Aldrich syndrome protein (N-WASP), Wiskott–Aldrich syndrome protein and SCAR homolog complex (WASH), WAS/WASL interacting protein family member 1 (WIP) and WAS protein family member 1 (WAVE) (10-14) activate the Arp2/3 complex in motile cells (15-17).

Focal adhesions are large macromolecular complexes that attach cells to the extracellular matrix through the transmembrane integrins (6, 18, 19). Recent studies suggest that myosin activation is involved in focal adhesion assembly. Myosin activation may generate contractile force to facilitate recruitment of various proteins to focal adhesions (6, 20-22). Furthermore, focal adhesion dimension and maturation are important for determining migratory speed (23, 24). ABL proto-oncogene 1, a non-receptor tyrosine kinase (c-Abl) regulates actin cytoskeletal reorganization essential for multiple cellular processes such as cell migration (1, 25-27), proliferation (1, 28, 29), cytokinesis (30), smooth muscle contraction (9, 31, 32), and cancer metastasis (26). c-Abl expression is upregulated in asthmatic human airway smooth muscle cells (31, 33). Inhibition of c-Abl by the inhibitor imatinib reduces airway hyperresponsiveness and remodeling in animal models of asthma (34), and relieves breathing difficulty of patients with severe asthma (4, 35).

In smooth muscle cells, c-Abl orchestrates actin reorganization by controlling glia maturation factor-γ (GMFγ)(36), which is a member of the ADF/cofilin depolymerizing factor superfamily (37-41). GMFγ is expressed in a variety of cell types including airway smooth muscle cells (36, 37, 39, 40). Unlike its relative cofilin, GMFγ does not interact directly with actin filaments, but rather binds specifically to two binding sites of the Arp2/3 complex to initiate actin branch disassembly and inhibit further nucleation (37, 41).

Previous loss-of-function studies have revealed the importance of GMFγ as a regulator of lamellipodia and overall migration (37, 38, 40). Furthermore, our group has previously shown that GMFγ undergoes phosphorylation at Tyr-104 in smooth muscle upon contractile activation. Tyr-104 is positioned within the Arp2 binding motif of GMFγ (36). GMFγ phosphorylation leads to its dissociation from the Arp2/3 complex and regulates actin dynamics (36).

In this study, we investigated the role of GMFγ phosphorylation at Tyr-104 in the coordination of both lamellipodial and focal adhesion dynamics through remodeling of actin during cell migration. We utilized high-resolution microscopy coupled with the 3D-reconstruction software Imaris 9.2.0 to identify quantitative changes in 3D-morphology of individual focal adhesions and actin architecture based on GMFγ functionality, which would otherwise be insufficient with a method of 2D-immunosfluorescent intensity analyses or co-immunoprecipitation (18). We unexpectedly identified a shift in GMFγ localization to either the leading edge or to growing focal adhesions. Phosphorylated GMFγ was localized to nascent adhesions near the leading edge and enhanced lamellipodial dynamics. Non-phosphorylated GMFγ was recruited to focal adhesions, induced maturation and inhibited cell migration. Furthermore, c-Abl regulates GMFγ spatial distribution, lamellipodial dynamics, and focal adhesion assembly.

METHODS

Cell Culture

Human airway smooth muscle cells (HASMCs) were prepared from bronchi and adjacent tracheas of control subjects (died from non-asthmatic causes) and patients (died from severe

AJRCMB Articles in Press. Published on 27-February-2019 as 10.1165/rcmb.2018-0352OC

asthma) obtained from the International Institute for Advanced Medicine (42). Non-asthmatic and asthmatic human airway smooth muscle cells were also obtained from Dr. Reynold A. Panettieri of Rutgers University (33). Human tissues were non-transplantable and consented for research. This study was approved by the Albany Medical College Committee on Research Involving Human Subjects. Details are provided in the online supplement.

Reagents and Transfection

Detailed plasmid sequences, lentiviral shRNA and primary antibody information are provided in the online supplement.

Transfections for migration assay were performed using FuGene HD Transfection Reagent (Promega Corporation Madison, WI). Transfections of cells for fixed and live-cell confocal microscopy were performed with Neon electroporation and Neon reagents (ThermoFisher MPK10025).

Western Blot and Co-Immunoprecipitation

Cells lysed with 2x SDS sample buffer boiled for 5 mins and separated onto SDS PAGE, then electro-transferred to nitrocellulose paper. Membranes were blocked using 2% bovine serum albumin (BSA) in PBS for 1hr and then probed with specific primary antibodies followed by horseradish peroxidase-conjugated secondary antibody (Fisher Scientific). Proteins were visualized using the Amersham Imager 600 (GE Healthcare). Additional Western Blot and Co-Immunoprecipitation information are detailed in the online supplement.

Immunofluorescence Microscopy

Imaging for fixed-cells and live-cells was conducted on a Zeiss LSM 880 NLO confocal microscope with Fast Airyscan module (Carl Zeiss Microscopy Jena, Germany) equipped with 63x oil 1.4 numerical aperture (NA) objective lens and collected through a 32-channel GaAsP

detector as 0.2 Airy units per channel. Z-stack collecting was under Nyquist sampling and with the fast airyscan SR settings. Live-cell imaging of GMFγ-GFP tagged mutants, Life-Act-RFP, and paxillin-mcherry constructs utilized the Fast-Airyscan module on the Zeiss LSM 880 confocal microscope. Microscope software used is the Zen Black 2 edition to process images for the Airyscan. Time-lapse microscopy was achieved by using a Leica A600 microscope with a 6-well incubator chamber hooked up to 5% CO_2. Additional detailed methods for Immunofluorescent Microscopy are found in online supplement.

Image Analysis

Detailed descriptions for image analysis are found in the online supplement.

Statistical Analysis

All data were analyzed using GraphPad Prism version 6.00 software (Windows, GraphPad Software, La Jolla, CA). A two-tailed one-way ANOVA followed by Tukey's multiple comparisons test was used for comparing Time-lapse microscopy parameters, lamellipodial protrusion/retraction velocity and events, comparing vinculin and zyxin area and number, all filament tracer experiments, and comparing the percent of GMFγ inside or outside adhesions (significance was determined by a $p<0.05$). A two-tailed Student's T-test was used to determine a significance of $p<0.05$ for knockdown cell focal adhesion parameters, protein level expression, and "wound" closure rates. A two-tailed Student's T-test was used to determine a significance of $p<0.05$ for blebbistatin-treated cells. Box and whisker plots and bar graphs were used to represent data shown. "n" denotes the number of individual cells, experiments, or objects rendered as stated within the text.

Results

Knockdown of GMFγ inhibits smooth muscle cell migration

AJRCMB Articles in Press. Published on 27-February-2019 as 10.1165/rcmb.2018-0352OC

To interrogate the function of GMFγ, we generated stable GMFγ knockdown in Human airway smooth muscle cells (HASMCs) by using lentiviral particles encoding control or GMFγ shRNA. Cells were serum-starved overnight before re-plating onto collagen-coated 6-well plates in 10% FBS/F12 medium. Migration of control or GMFγ knockdown cells was monitored live by time-lapse microscopy and analyzed using the NIH ImageJ software. Cells undergoing cell proliferation over the course of the experiment were not chosen for analysis. GMFγ knockdown diminished the speed and accumulated distance of motile HASMCs (Figure 1, A, B, F, G, Movie 1). Immunoblot analysis verified effective knockdown in cells expressing GMFγ shRNA by 80% (Figure S1A). We also performed a wound-healing assay to assess the effects of GMFγ knockdown on directed cell migration (Figure S1B). Loss of GMFγ led to a decrease in the ability of cells to close the scratch area in 12 hrs as compared to control shRNA expressing cells (Figure S1C). Furthermore, we re-expressed GMFγ in the knockdown cells using the experimental procedures as we previously described (36) (Figure S1, D-F). Rescue of GMFγ restored the speed and distance of migratory cells (Figure 1, A-C, F, G) (Movie 1).

GMFγ phosphorylation at Y104 regulates smooth muscle cell migration

Since GMFγ has a role in regulating smooth muscle contraction, we evaluated the role of GMFγ phosphorylation at this residue in cell migration. We engineered EGFP-tagged non-phosphorylated mutant (Y104F) GMFγ (substitution of phenylalanine at Y104) and phosphorylation mimic mutant (Y104D) GMFγ (aspartic acid substitution at Y104) (36). These DNA constructs were transiently transfected into GMFγ knockdown cells (Figure S1, D-F) and migration of live-cells was monitored by time-lapse microscopy. (Figure 1 A-E, Movie 1). The expression of Y104F-GMFγ in the knockdown cells did not recover

cell migration (Figure 1, D, F, G). However, the expression of Y104D-GMFγ in the knockdown cells restored the speed and distance of motile cells (Figure 1, E, F, G). These results suggest GMFγ phosphorylation contributes to the regulation of cell migration.

Knockdown of GMFγ disrupts N-WASP (pY256) spatial distribution and reduces focal adhesion area

Since speed and distance were attenuated by knockdown of GMFγ, we evaluated the spatial distribution of GMFγ in smooth muscle cells with a focus on lamellipodia and lamella (dynamic cell front during migration). GMFγ was localized on the cell leading edge of the lamellipodia (Figure 2A). Moreover, merged z-slice confocal images showed that a pool of GMFγ was colocalized with vinculin, a marker of focal adhesions. To our knowledge this is the first evidence of GMFγ localization to the focal adhesion compartment. In addition, active N-WASP has been implicated in cell migration (10, 13), we also examined the cellular location of N-WASP (pY256) in motile cells. N-WASP was distributed both in focal adhesions and the leading edge (Figure 2A). Furthermore, co-immunoprecipitation analysis was used to assess interaction of GMFγ with vinculin and N-WASP (pY256). Vinculin and N-WASP (pY256) were found in GMFγ immunoprecipitates (Figure 2B). Conversely, GMFγ and N-WASP (pY256) were found in vinculin precipitates (Figure 2B) suggesting association of GMFγ with vinculin and N-WASP (pY256).

To determine whether GMFγ affects focal adhesions and the actin-regulatory proteins, we assessed the effects of GMFγ knockdown on focal adhesion size and distribution of N-WASP (pY256). Focal adhesions within human airway smooth muscle cells span

AJRCMB Articles in Press. Published on 27-February-2019 as 10.1165/rcmb.2018-0352OC

multiple Airyscan z-slices, therefore, to quantify morphological changes we used the Imaris 3D object-based rendering software (Figure S2, S3 A-F and *Methods*) to reconstruct vinculin into 3D-objects using the surface module because of its ability to accurately quantify focal adhesion size and distribution changes by surface area and distance transformation, two MatLab algorithms (18, 43) (Figure S3). We also reconstructed the punctate immunostaining of N-WASP (pY256) into spots using the spot module of the Imaris software. 3D-surfaces and spots are reconstructed based on immunofluorescent intensity, surface area, and quality of rendering, to identify morphological parameters and interaction between objects in 3D (18, 43). Knockdown of GMFγ caused a significant decrease in vinculin surface area without impacting individual vinculin numbers as compared to control cells (Figure 2, C, E, F). We also observed a significant decrease in the enrichment of N-WASP (pY256) with vinculin in GMFγ knockdown cells (Figure 2, C, G). Altogether, these results suggest that GMFγ is localized within focal adhesions and that it may regulate focal adhesion growth through the recruitment of N-WASP (pY256).

We further examined whether N-WASP localization was also disrupted by GMFγ knockdown at the leading edge of the lamellipodia (Figure 2D and Figure S3, G-I). Knockdown of GMFγ led to a decrease in Arp2 colocalized with N-WASP (pY256) at the leading edge as compared to cells expressing control shRNA (Figure 2D, H).

GMFγ phosphorylation at Y104 impacts focal adhesion dynamics in live cells

During migration, focal adhesions undergo dynamic changes to accommodate alterations in surroundings (1). We next sought to determine if the phosphorylation state of GMFγ

affects focal adhesion dynamics in live-cells by observing mCherry-labeled paxillin, a focal adhesion-associated protein that also interacts with vinculin in both nascent and mature adhesions (21). Cells were co-transfected with WT, Y104F, or Y104D-GMFγ and mcherry-paxillin. Labeled paxillin images of cells were monitored live by fast Airyscan microscopy (Figure S4, A-C, Movie 2). Images were taken every 30-seconds over the course of a 20-minute period with a sampling of 4 z-slices. Imaris software with surface module package was utilized to 3D reconstruct paxillin surface area based on fluorescent intensity, quality, area, and track duration (minimum of 300 seconds in length) (*Methods*). The surface area of each paxillin object (WT-GMFγ n=1,489, Y104F-GMFγ n=2,012, Y104D-GMFγ n=2,387) was tracked over time for each sample (n=10 individual cells). Representative regions of interest (ROI's) were graphed to demonstrate focal adhesion dynamics (Figure S4, A-C). WT-GMFγ expressing cells exhibited an initial increase in paxillin surface area, which peaked at an average of 6.73um^2 (SD = +/- 2.44), followed by a decrease in surface area (Figure S4, A, D, E). Several focal adhesions did display stability in our WT-GMFγ expressing cells but averaged a consistent area of 8um^2 (SD = +/- 1.67). Conversely, Y104F-GMFγ expressing cells displayed large stable paxillin focal adhesions, which remained at an average of 14.1um^2 (SD = +/- 6.22) throughout the duration of imaging (Figure S4, B, D, E). Unexpectedly, during the period of imaging, we did not observe turnover of any of these focal adhesions (Figure S4 B). In addition, expression of Y104D-GMFγ revealed a similar trend to WT-GMFγ expressing cells but was limited in the growth of paxillin focal adhesions averaging a peak surface area of 3.36um^2 (SD = +/- 0.784) (Figure S4 C, D, E). However, there were several occurrences of focal adhesions that did not disassemble in the time frame but again were limited to an

AJRCMB Articles in Press. Published on 27-February-2019 as 10.1165/rcmb.2018-0352OC

average area of 3.41um^2 (SD = +/- 1.23) (Figure S4 D). Quantification analysis showed that average peak of paxillin surface area was higher in cells expressing Y104F-GMFγ than in cells expressing WT or Y104D-GMFγ (Figure S4 E). These results suggest that GMFγ phosphorylation regulates the dynamics of focal adhesions.

Phosphorylation at Y104 regulates focal adhesion clustering and GMFγ distribution

Because we observed knockdown of GMFγ decreased vinculin clustering, we asked whether the phosphorylation state of GMFγ affects focal adhesion assembly by expressing phosphorylation-modified GMFγ mutants in GMFγ KD cells. Cells expressing EGFP-tagged WT-, Y104F- or Y104D-GMFγ were plated on coverslips followed by immunostaining for vinculin and zyxin (Figure 3A). Zyxin is a marker for mature focal adhesions (44). Imaris software was used to analyze number and surface area of focal adhesions (Figure S5 and *Methods*). Expression of Y104F-GMFγ increased the number and area of vinculin surfaces as compared to cells expressing WT-GMFγ (Figure 3, A-C). In contrast, introduction of Y104D-GMFγ did not increase the number and area of vinculin surfaces when compared to cells expressing WT-GMFγ (Figure 3, A-C). In fact, expression of Y104D-GMFγ decreased the area of vinculin surfaces by 1 μm^2, but significantly (Figure 3, A-C). Furthermore, expression of Y104F-GMFγ increased the number of zyxin surface without affecting the surface area of zyxin (Figure 3, D and E). Y104D-GMFγ did not affect the number and area of zyxin surfaces (Figure 3, D and E). These results suggest that lower phosphorylation of GMFγ at this residue promotes focal adhesion clustering and recruitment of zyxin to adhesions.

We also examined the spatial distribution of WT and mutant GMFγ in HASM cells (Figure 3F, Figure S5 A-E and *Methods*). Imaris software was utilized to separate populations of GMFγ based on the proximity to vinculin and zyxin markers within lamellipodia (Figure 3F). We unexpectedly found that phosphorylation state of GMFγ affected its distribution in focal adhesions. Approximately 68% of Y104F-GMFγ were found inside focal adhesions as compared to WT-GMFγ (36%). In contrast, 16% of Y104D-GMFγ were localized inside focal adhesions (Figure 3G). Moreover, 32% of Y104F-GMFγ, 64% of WT-GMFγ, and 84% of Y104D-GMFγ were positioned outside of focal adhesions (Figure 3G).

Next, we used Imaris software to further analyze detailed distribution of GMFγ and its mutants within individual focal adhesions (Figure 3F, Figure S5, A-E and *Methods*). This method allowed for separation of GMFγ populations associated with vinculin or zyxin reconstructed surfaces, nascent and mature adhesions respectively. 47% of WT-GMFγ localized with nascent adhesions whereas 53% of WT-GMFγ contacted mature adhesions (Figure 3H). However, Y104F-GMFγ largely (74%) associated with mature adhesions with only 26% Y104F-GMFγ within nascent adhesions (Figure 3H). Moreover, 60% of Y104D-GMFγ localized to nascent adhesions with 40% of Y104D-GMFγ within mature adhesions (Figure 3H). These results suggest that non-phosphorylated GMFγ largely contacts zyxin-associated mature adhesions whereas phosphorylated GMFγ localizes with nascent vinculin-only adhesions.

Actin architecture and connection of actin fibers to vinculin and are regulated by GMFγ phosphorylation at Y104

AJRCMB Articles in Press. Published on 27-February-2019 as 10.1165/rcmb.2018-0352OC

Because GMFγ phosphorylation was found to affect focal adhesion clustering, we asked whether GMFγ Y104 phosphorylation affects actin architecture by assessing the effects of non-phosphorylated or phosphorylated mutant on F-actin structure in lamellipodia. Cells were co-transfected with constructs for WT-, Y104F-, or Y104D-GMFγ and LifeAct-RFP plasmid, which generates a 17-amino acid peptide to visualize F-actin followed by immunostaining for vinculin. Fast Airyscan microscopy and Imaris software with filament tracer package were used to evaluate actin architecture (*Methods*). In cells treated with WT-GMFγ, actin fibers displayed both a linear structure and an actin meshwork within lamellipodia. In contrast, actin fibers of cells expressing Y104F-GMFγ showed asterisk-like topology characterized by nucleation centers and arm-like radially orientated F-actin strands. Moreover, cells expressing Y104D-GMFγ displayed a majority of actin meshwork architecture (Figure 4A). Furthermore, the expression of Y104F-GMFγ increased actin fibers contacting vinculin (Figure 4B), reduced actin fiber branching (Figure 4C), and enhanced the occurrence of actin asters (Figure 4D). Moreover, the expression of Y104D-GMFγ increased vinculin-associated actin fibers (Figure 4B) and actin fiber branches (Figure 4C), and reduced actin asters (Figure 4C). These findings suggest that GMFγ phosphorylation at this residue regulates the reorganization of the actin cytoskeleton and the interaction of actin fibers with focal adhesions.

GMFγ phosphorylation at Y104 modulates lamellipodial dynamics

During migration, cells undergo cyclic extension and retraction of lamellipodia to facilitate cell movement forward (1, 5, 8). We also evaluated the role of GMFγ phosphorylation in lamellipodial dynamics. Cells expressing WT-, Y104F-, or Y104D-GMFγ were transfected with LifeAct-RFP to monitor changes in lamellipodial dynamics using Fast Airyscan

microscope. To analyze lamellipodial dynamics, we used an ImageJ plugin known as "automated detection and analysis of protrusions" (ADAPT) (45) (*Methods*). Expression of Y104F-GMFγ severely impaired protrusion velocity, as well as retraction velocity as compared to cells expressing WT-GMFγ (Figure S6, A-C; Movie 3). Moreover, actin asters were also observed, but dynamic in live cells expressing Y104F-GMFγ (Figure S6A, Movie 3). However, expression of Y104D-GMFγ recovered protrusion velocity and retraction velocity (Figure S6, A-C, Movie 3). Furthermore, expression of Y104F-GMFγ reduced protrusion events and enhanced retraction events as compared to cells expressing WT-GMFγ. However, expression of Y104D-GMFγ restored these events (Figure S6, A, D, E). Together these data suggest the phosphorylation of GMFγ can modulate the actin cytoskeleton to promote efficient lamellipodial dynamics.

Myosin activation regulates the recruitment of GMFγ to focal adhesions

As described earlier, GMFγ phosphorylation affects its distribution in focal adhesions (Figure 3). Because myosin activity has been implicated in the recruitment of focal adhesion-associated proteins and focal adhesion morphology (6, 21, 22), we examined whether myosin activation influences GMFγ distribution. Cells expressing WT-GMFγ, Y104F-GMFγ or Y104D-GMFγ were seeded on coverslips followed by treatment with blebbistatin, a small molecule inhibitor of myosin II ATPase activity (46). Cells were then immunofluorescently stained for vinculin (Figure 5A). Approximately 30% of WT-GMFγ contacted vinculin, whereas 60% of Y104F-GMFγ and around 10% of Y104D-GMFγ associated with vinculin (Figure 5B). Treatment with blebbistatin reduced the populations of WT-GMFγ and Y104F-GMFγ contacting vinculin. Moreover, blebbistatin treatment increased the population of Y104D-GMFγ contacting vinculin (Figure 5B). Furthermore,

AJRCMB Articles in Press. Published on 27-February-2019 as 10.1165/rcmb.2018-0352OC

treatment with blebbistatin diminished the area of vinculin surfaces in cells expressing WT-GMFγ and Y104F-GMFγ, but not Y104D-GMFγ (Figure 5, B, C). These results suggest that myosin activity affects phosphorylation-dependent GMFγ recruitment to focal adhesion and focal adhesion morphology.

Because c-Abl is known to catalyze GMFγ Y104 phosphorylation (36), we assessed the role of myosin activity in c-Abl phosphorylation at Y412, an indication of c-Abl activity as well as GMFγ phosphorylation at Y104 (25). Treatment with blebbistatin inhibited both c-Abl phosphorylation and GMFγ phosphorylation (Figure 5, D, E). Moreover, we verified that blebbistatin treatment reduced myosin light chain-20 phosphorylation (Figure 5, D, E).

c-Abl regulates the accumulation of GMFγ to focal adhesions of migrating cells

Next, we assessed whether c-Abl affects the spatial distribution of GMFγ in motile cells. Cells expressing control shRNA and c-Abl knockdown cells were generated by the methods previously described (30), and immunostained for GMFγ, N-WASP (pY256), zyxin, and vinculin. c-Abl knockdown resulted in increases in the number and surface area of vinculin (Figure S7, A, C, D) and zyxin (Figure S7, B, E, F). Furthermore, we used Imaris software with surface module package to analyze the localization of GMFγ and N-WASP (pY256) in vinculin or zyxin adhesions (*Methods*). Knockdown of c-Abl enhanced localization of GMFγ spots with vinculin surfaces from 30% to 48% (Figure S7 G). Localization of N-WASP (pY256) spots with vinculin surfaces was also higher in c-Abl knockdown cells (Figure S7, H). Moreover, contact of GMFγ and N-WASP (pY256) with zyxin was higher in c-Abl knockdown cells compared to control cells (Figure S7, I, J).

GMFγ phosphorylation is involved in faster migration of human HASMCs

Because airway smooth muscle cell motility has been implicated in airway remodeling of asthma (1, 3, 4), and our present results demonstrated a role of GMFγ phosphorylation in cell migration, we assessed whether GMFγ and its phosphorylated form are altered in asthma. Immunoblot analysis showed that total and phosphorylated GMFγ was upregulated in asthmatic HASMCs (Figure 6, A, B). Moreover, speed and accumulated distance were increased in asthmatic HASMCs (Figure 6, C, D, F, G). More importantly, the expression of Y104F-GMFγ inhibited migration of asthmatic HASMCs (Figure 6, E, F, G).

Discussion

GMFγ is highly expressed in HASMCs (36). Our present study suggests that GMFγ is an important molecule that regulates cell migration. GMFγ deficiency reduced active N-WASP recruitment to focal adhesions and inhibited focal adhesion formation (Figure 2). This may be because GMFγ can bind the C-terminus of N-WASP (37) to facilitate their interaction. N-WASP and its associated proteins are known to modulate focal adhesion assembly (12). Furthermore, GMFγ deficiency reduced the activation of the Arp2/3 complex in the leading edge. Again, this could be due to the ability of GMFγ to interact with Arp2 and N-WASP (37).

Our experimental and quantitative results suggest a model for how GMFγ phosphorylation can regulate lamellipodial and focal adhesion dynamics during airway smooth muscle cell migration (Figure 7). Localization of phospho-GMFγ at the leading edge increased the recruitment of N-WASP (pY256) to promote Arp2/3-mediated actin branching at the cell

AJRCMB Articles in Press. Published on 27-February-2019 as 10.1165/rcmb.2018-0352OC

front, as indicated by presence of actin branched organization within protrusions (Figures 4, 7), which may increase lamellipodial extension (Figure S6). Phosphorylation at Y-104 promotes dissociation of GMFγ from Arp2 (36). Thus, it is possible that the released GMFγ may facilitate N-WASP recruitment to the leading edge. Several studies have identified an important connection between branched actin and the formation of nascent adhesions in an Arp2/3-dependent manner (16, 17, 19). We hypothesized that GMFγ phosphorylation may promote a switch in actin organization to regulate focal adhesion morphology (Figure 7). We observed a change in actin organization between branched to linear actin as non-phosphorylated GMFγ was enriched in mature focal adhesions (Figures 3 and 4). Our results suggest that non-phosphorylated GMFγ promotes aster actin formation that may enhance focal adhesion maturation and stability leading to a dramatic reduction in cell migratory speed (Figures 1, 3 and 4). This is because focal adhesion maturation and size affect cell migration (23). In addition, aster actin may change membrane structure (43), and inhibit protrusion extension and cell migration (Figures 1, 4, S4, S6). The formation of geodesic-actin organization (actin asters) has previously been reported in cells undergoing topological stress (47, 48) and could form through actin nodes containing the formin, disheveled-associated activator of morphogenesis 1 (DAAM1), the crosslinker filamin A (FlnA) and myosin II filaments (49).

Our studies on phospho-mimetic Y104D-GMFγ suggest that increased actin fiber branching separates focal adhesions into smaller units within protrusions of migrating cells. Recently, a study found that focal adhesions undergo splitting events into multiple focal adhesion units of uniform width that are laterally associated through actin filaments generated by actin-assembly proteins adenomatosis polyposis coli (APC) protein and

vasodilator-stimulated phosphoprotein(VASP) (18). These events were found to occur under increased actin tension driven by myosin II activity (18).

During cell migration, c-Abl phosphorylation and activation at the leading edge can be initiated by β1 integrin and growth factor (1). In this manuscript, phosphorylated GMFγ localized to the leading edge. c-Abl KD inhibits GMFγ phosphorylation. Thus, β1 integrin and growth factors are important initiators for GMFγ mediated processes during migration.

The molecular mechanism for the directed translocation of phosphorylated GMFγ between the leading edge and focal adhesions remains unknown. Here, we demonstrate that the enrichment of non-phosphorylated GMFγ within focal adhesions is driven by myosin II activity, as blebbistatin treatment attenuated GMFγ enrichment with vinculin (Figure 5). Myosin activation is also involved in the recruitment of other focal adhesion-associated proteins (6). Myosin activation may induce filament contraction and promote protein accumulation in the adhesive structure. However, other possibilities may also exist. One study in macrophages suggests that GMFγ may play a role in β1 integrin recycling back to the leading edge through interaction with syntaxin-4 (STX4) and syntaxin-binding protein 4 (STXBP4), two proteins involved with vesicle trafficking and fusion to the plasma membrane (40). In addition, previous studies have revealed that cofilin-1, a homologous actin depolymerizing factor to GMFγ, interacts with high affinity to membrane phospholipids PI(4,5)P2, PI(3,4)P2, and PI(3,4,5)P3 through electrostatic interactions (50). Phospholipid composition and clustering on vesicles may recruit and bind phosphorylated GMFγ, thus transporting GMFγ to the leading edge. Furthermore, a homologous actin depolymerizing factor Abp1 (actin-binding protein 1) was found to

AJRCMB Articles in Press. Published on 27-February-2019 as 10.1165/rcmb.2018-0352OC

regulate vesicle trafficking by interacting with distinct Golgi membrane regions (39). Abp1 was shown in yeast to enhance actin polymerization by interacting with both N-WASP and Arp2/3 (39). Abp1 can also bind endocytic proteins such as myosin Vb and synaptojanin to connect vesicle recycling with dynamic cortical actin (39). Moreover, Arp2/3-mediated actin polymerization on the endosomal membrane surface was critical for integrin recycling back to the plasma membrane (7). Future studies are needed to test these possibilities in the context of cell migration.

We additionally observed that c-Abl activation was myosin-dependent as treatment of blebbistatin decreased c-Abl phosphorylation at Y-412, a marker of c-Abl catalytic activity, as well as GMFγ phosphorylation at Y-104 (Figure 5). c-Abl and its isoform Arg have been reported to interact with integrins and focal adhesion-associated proteins (14, 26), as well as promote actin formation (27). Our image analysis showed a dramatic shift in localization of Y104D-GMFγ outside of adhesions, suggesting c-Abl phosphorylation might liberate GMFγ from the adhesions upon increased mechanical tension. c-Abl may act as a switch to promote changes in actin organization needed to control focal adhesion growth and subsequent actin branch formation within protrusions by regulating GMFγ localization during cell migration (Figure 7).

Our results suggest that GMFγ phosphorylation at Y-104 is involved in asthma pathogenesis as evidenced by higher expression of phosphorylated and total GMFγ, and inhibition of asthmatic cell migration by non-phosphorylated GMFγ mutant. Furthermore, our previous studies show that c-Abl expression is higher in airway smooth muscle cells from patients with asthma and from animal models of asthma (31, 33). Thus, the c-Abl-

GMFγ pathway may contribute to increased airway smooth muscle cell migration during asthma progression.

In summary, our study provides novel insight into the critical role of GMFγ phosphorylation in regulating lamellipodial and focal adhesion dynamics, important for directed HASMCs migration (Figure 7). Phosphorylation of GMFγ by c-Abl non-receptor tyrosine kinase and myosin contractility are determinants for GMFγ spatial localization to the leading edge and growing focal adhesions respectively (Figure. 7). Localization of phospho-GMFγ at the leading-edge leads to increased N-WASP (pY256) enrichment, Arp2 activation and increased protrusion extension, whereas localization of non-phosphorylated GMFγ within focal adhesion promoted N-WASP (pY256) recruitment, actin re-organization, focal adhesion clustering and recruitment of zyxin (Figure 7). Thus, we propose that GMFγ localization and phosphorylation state is an important modulatory switch that controls actin organization and focal adhesion dynamics to promote cell migration.

ACKNOWLEDGEMENTS

This work was supported by NHLBI grants HL-110951, HL-113208, and HL-130304 from the National Institutes of Health (to Dale D. Tang). Also, this work was supported by the American Heart Association predoctoral fellowship: 16PRE31430001 (to Brennan D. Gerlach). We acknowledge Dr. Gabrielle Fredman for assisting in editing manuscript. We acknowledge the Albany Medical College Imaging Core and Dr. J. Mazurkiewicz for helping us with the Zeiss LSM 880, and Imaris software.

AJRCMB Articles in Press. Published on 27-February-2019 as 10.1165/rcmb.2018-0352OC

References

1. Tang DD, Gerlach BD. The roles and regulation of the actin cytoskeleton, intermediate filaments and microtubules in smooth muscle cell migration. *Respir Res* 2017;18(1):54.
2. Salter B, Pray C, Radford K, Martin JG, Nair P. Regulation of human airway smooth muscle cell migration and relevance to asthma. *Respir Res* 2017;18(1):156.
3. Gizycki MJ, Adelroth E, Rogers AV, O'Byrne PM, Jeffery PK. Myofibroblast involvement in the allergen-induced late response in mild atopic asthma. *Am J Respir Cell Mol Biol* 1997;16(6):664-673.
4. Kaminska M, Foley S, Maghni K, Storness-Bliss C, Coxson H, Ghezzo H, Lemiere C, Olivenstein R, Ernst P, Hamid Q, et al. Airway remodeling in subjects with severe asthma with or without chronic persistent airflow obstruction. *J Allergy Clin Immunol* 2009;124(1):45-51 e41-44.
5. Krause M, Gautreau A. Steering cell migration: Lamellipodium dynamics and the regulation of directional persistence. *Nat Rev Mol Cell Biol* 2014;15(9):577-590.
6. Burridge K, Guilluy C. Focal adhesions, stress fibers and mechanical tension. *Exp Cell Res* 2016;343(1):14-20.
7. Pizarro-Cerda J, Chorev DS, Geiger B, Cossart P. The diverse family of arp2/3 complexes. *Trends Cell Biol* 2017;27(2):93-100.
8. Pollard TD, Borisy GG. Cellular motility driven by assembly and disassembly of actin filaments. *Cell* 2003;112(4):453-465.
9. Tang DD. The dynamic actin cytoskeleton in smooth muscle. *Adv Pharmacol* 2018;81:1-38.
10. Burianek LE, Soderling SH. Under lock and key: Spatiotemporal regulation of wasp family proteins coordinates separate dynamic cellular processes. *Semin Cell Dev Biol* 2013;24(4):258-266.
11. Chen B, Brinkmann K, Chen Z, Pak CW, Liao Y, Shi S, Henry L, Grishin NV, Bogdan S, Rosen MK. The wave regulatory complex links diverse receptors to the actin cytoskeleton. *Cell* 2014;156(1-2):195-207.
12. Ramesh N, Massaad MJ, Kumar L, Koduru S, Sasahara Y, Anton I, Bhasin M, Libermann T, Geha R. Binding of the wasp/n-wasp-interacting protein wip to actin regulates focal adhesion assembly and adhesion. *Molecular and cellular biology* 2014;34(14):2600-2610.
13. Sun Y, Leong NT, Jiang T, Tangara A, Darzacq X, Drubin DG. Switch-like arp2/3 activation upon wasp and wip recruitment to an apparent threshold level by multivalent linker proteins in vivo. *Elife* 2017;6.
14. Miller MM, Lapetina S, MacGrath SM, Sfakianos MK, Pollard TD, Koleske AJ. Regulation of actin polymerization and adhesion-dependent cell edge protrusion by the abl-related gene (arg) tyrosine kinase and n-wasp. *Biochemistry* 2010;49(10):2227-2234.
15. Swaney KF, Li R. Function and regulation of the arp2/3 complex during cell migration in diverse environments. *Curr Opin Cell Biol* 2016;42:63-72.
16. Duleh SN, Welch MD. Regulation of integrin trafficking, cell adhesion, and cell migration by wash and the arp2/3 complex. *Cytoskeleton (Hoboken)* 2012;69(12):1047-1058.

17. Serrels B, Serrels A, Brunton VG, Holt M, McLean GW, Gray CH, Jones GE, Frame MC. Focal adhesion kinase controls actin assembly via a ferm-mediated interaction with the arp2/3 complex. *Nat Cell Biol* 2007;9(9):1046-1056.
18. Young LE, Higgs HN. Focal adhesions undergo longitudinal splitting into fixed-width units. *Current biology : CB* 2018;28(13):2033-2045 e2035.
19. Chorev DS, Moscovitz O, Geiger B, Sharon M. Regulation of focal adhesion formation by a vinculin-arp2/3 hybrid complex. *Nat Commun* 2014;5:3758.
20. Maiuri P, Rupprecht J-F, Wieser S, Ruprecht V, Bénichou O, Carpi N, Coppey M, De Beco S, Gov N, Heisenberg C-P, et al. Actin flows mediate a universal coupling between cell speed and cell persistence. *Cell* 2015;161(2):374-386.
21. Zhou DW, Lee TT, Weng S, Fu J, Garcia AJ. Effects of substrate stiffness and actomyosin contractility on coupling between force transmission and vinculin-paxillin recruitment at single focal adhesions. *Mol Biol Cell* 2017;28(14):1901-1911.
22. Carisey A, Tsang R, Greiner AM, Nijenhuis N, Heath N, Nazgiewicz A, Kemkemer R, Derby B, Spatz J, Ballestrem C. Vinculin regulates the recruitment and release of core focal adhesion proteins in a force-dependent manner. *Current biology : CB* 2013;23(4):271-281.
23. Kim DH, Wirtz D. Focal adhesion size uniquely predicts cell migration. *FASEB J* 2013;27(4):1351-1361.
24. Kim D-H, Wirtz D. Predicting how cells spread and migrate: Focal adhesion size does matter. *Cell Adhesion & Migration* 2013;7(3):293-296.
25. Woodring PJ. Regulation of f-actin-dependent processes by the abl family of tyrosine kinases. *Journal of Cell Science* 2003;116(13):2613-2626.
26. Smith-Pearson PS, Greuber EK, Yogalingam G, Pendergast AM. Abl kinases are required for invadopodia formation and chemokine-induced invasion. *J Biol Chem* 2010;285(51):40201-40211.
27. Cleary RA, Wang R, Waqar O, Singer HA, Tang DD. Role of c-abl tyrosine kinase in smooth muscle cell migration. *Am J Physiol Cell Physiol* 2014;306(8):C753-761.
28. Jia L, Wang R, Tang DD. Abl regulates smooth muscle cell proliferation by modulating actin dynamics and erk1/2 activation. *Am J Physiol Cell Physiol* 2012;302(7):C1026-1034.
29. Wang R, Mercaitis OP, Jia L, Panettieri RA, Tang DD. Raf-1, actin dynamics, and abelson tyrosine kinase in human airway smooth muscle cells. *Am J Respir Cell Mol Biol* 2013;48(2):172-178.
30. Chen S, Tang DD. C-abl tyrosine kinase regulates cytokinesis of human airway smooth muscle cells. *Am J Respir Cell Mol Biol* 2014;50(6):1076-1083.
31. Cleary RA, Wang R, Wang T, Tang DD. Role of abl in airway hyperresponsiveness and airway remodeling. *Respir Res* 2013;14:105.
32. Wang R, Cleary RA, Wang T, Li J, Tang DD. The association of cortactin with profilin-1 is critical for smooth muscle contraction. *J Biol Chem* 2014;289(20):14157-14169.
33. Liao G, Panettieri RA, Tang DD. Microrna-203 negatively regulates c-abl, erk1/2 phosphorylation, and proliferation in smooth muscle cells. *Physiol Rep* 2015;3(9).
34. Rhee CK, Kim JW, Park CK, Kim JS, Kang JY, Kim SJ, Kim SC, Kwon SS, Kim YK, Park SH, et al. Effect of imatinib on airway smooth muscle thickening in a murine

AJRCMB Articles in Press. Published on 27-February-2019 as 10.1165/rcmb.2018-0352OC

model of chronic asthma. *International archives of allergy and immunology* 2011;155(3):243-251.
35. Cahill KN, Katz HR, Cui J, Lai J, Kazani S, Crosby-Thompson A, Garofalo D, Castro M, Jarjour N, DiMango E, et al. Kit inhibition by imatinib in patients with severe refractory asthma. *N Engl J Med* 2017;376(20):1911-1920.
36. Wang T, Cleary RA, Wang R, Tang DD. Glia maturation factor-gamma phosphorylation at tyr-104 regulates actin dynamics and contraction in human airway smooth muscle. *Am J Respir Cell Mol Biol* 2014;51(5):652-659.
37. Goode BL, Sweeney MO, Eskin JA. Gmf as an actin network remodeling factor. *Trends Cell Biol* 2018;28(9):749-760.
38. Poukkula M, Hakala M, Pentinmikko N, Sweeney MO, Jansen S, Mattila J, Hietakangas V, Goode BL, Lappalainen P. Gmf promotes leading edge dynamics and collective cell migration in vivo. *Current biology : CB* 2014;24(21):2533.
39. Poukkula M, Kremneva E, Serlachius M, Lappalainen P. Actin-depolymerizing factor homology domain: A conserved fold performing diverse roles in cytoskeletal dynamics. *Cytoskeleton (Hoboken)* 2011;68(9):471-490.
40. Aerbajinai W, Liu L, Zhu J, Kumkhaek C, Chin K, Rodgers GP. Glia maturation factor-gamma regulates monocyte migration through modulation of beta1-integrin. *J Biol Chem* 2016;291(16):8549-8564.
41. Luan Q, Nolen BJ. Structural basis for regulation of arp2/3 complex by gmf. *Nat Struct Mol Biol* 2013;20(9):1062-1068.
42. Li J, Wang R, Gannon OJ, Rezey AC, Jiang S, Gerlach BD, Liao G, Tang DD. Polo-like kinase 1 regulates vimentin phosphorylation at ser-56 and contraction in smooth muscle. *J Biol Chem* 2016;291(45):23693-23703.
43. Fritzsche M, Li D, Colin-York H, Chang VT, Moeendarbary E, Felce JH, Sezgin E, Charras G, Betzig E, Eggeling C. Self-organizing actin patterns shape membrane architecture but not cell mechanics. *Nat Commun* 2017;8:14347.
44. Uemura A, Nguyen TN, Steele AN, Yamada S. The lim domain of zyxin is sufficient for force-induced accumulation of zyxin during cell migration. *Biophys J* 2011;101(5):1069-1075.
45. Barry DJ, Durkin CH, Abella JV, Way M. Open source software for quantification of cell migration, protrusions, and fluorescence intensities. *J Cell Biol* 2015;209(1):163-180.
46. Kolega J. Phototoxicity and photoinactivation of blebbistatin in uv and visible light. *Biochem Biophys Res Commun* 2004;320(3):1020-1025.
47. Bermudez JY, Montecchi-Palmer M, Mao W, Clark AF. Cross-linked actin networks (clans) in glaucoma. *Exp Eye Res* 2017;159:16-22.
48. Entcheva E, Bien H. Mechanical and spatial determinants of cytoskeletal geodesic dome formation in cardiac fibroblasts. *Integr Biol (Camb)* 2009;1(2):212-219.
49. Luo W, Lieu ZZ, Manser E, Bershadsky AD, Sheetz MP. Formin daam1 organizes actin filaments in the cytoplasmic nodal actin network. *PLoS One* 2016;11(10):e0163915.
50. Zhao H, Hakala M, Lappalainen P. Adf/cofilin binds phosphoinositides in a multivalent manner to act as a pip(2)-density sensor. *Biophys J* 2010;98(10):2327-2336.

Figure Legends

Figure 1: GMFγ phosphorylation at Y104 regulates smooth muscle cell migration (A-E). Time-lapse microscopy was used to track human airway smooth muscle cells (HASMCs) expressing control shRNA and GMFγ shRNA, as well as cells transfected with WT-GMFγ, Y104F-GMFγ, and Y104D-GMFγ plasmids. Images were taken every 10 minutes for 16 hours. Migration plots generated by Image J plugin display migration patterns for each cell type. **(F, G).** Graphical comparisons represent the calculated speed and accumulated distance for each cell type. Two-tailed one-way ANOVA with Tukey's post hoc test was used (*p<0.05, Control shRNA n=51, GMFγ KD n=41, WT-GMFγ n=27, Y104F-GMFγ n=45, Y104D-GMFγ n=31 n = pooled cell numbers from 4 non-asthmatic human donors).

Figure 2: Knockdown of GMFγ disrupts N-WASP (pY256) spatial distribution and reduces focal adhesion area. **(A)** HASMCs were plated on collagen-I coated coverslips and immunostained for total GMFγ, N-WASP (pY256), and Vinculin. Z-slice images were taken on Zeiss LSM880 confocal microscope with Fast Airyscan module using 488nm, 561nm, and 633nm lasers. White scale bar = 5um and zoomed-in = 2um. Arrowheads point to focal adhesions and Arrows point to leading edge. Representative image from n=10 individual cells. **(B)** Co-immunoprecipitation assay was performed on HASMCs using antibodies targeting endogenous GMFγ or vinculin. Co-IP samples were loaded and separated on an SDS PAGE gel, where they were electro-transferred onto nitrocellulose paper and immunoblotted with primary antibodies for vinculin, N-WASP (pY256), Arp2, and GMFγ. Representative immunoblot from n=4 independent experiments. **(C)** Control shRNA or GMFγ knockdown expressing cells were immunostained for N-WASP (pY256) and vinculin. Z-slice images were taken on Zeiss LSM880 confocal microscope with Fast Airyscan module, white scale bar = 5um, zoomed-in = 2um. White line denotes the leading edge. Arrowheads point to focal adhesions. **(D)** Control shRNA or GMFγ knockdown expressing cells were immunostained for Arp2 and N-WASP (pY256). Arrows point to leading edge. **(E-G)** Imaris 9.1.2 software was used to 3D-render spots (Control shRNA= 18,433, GMFγ KD= 21,163) and surfaces (Control shRNA= 1,993, GMFγ KD= 2,121) for quantitative analysis of vinculin number, area, and percent N-WASP spots contacting vinculin surfaces from 10 individual cells (Fig. S3 and Methods). **(H)** Imaris 9.1.2 software was used to quantify the percent Arp2 spots (Control shRNA= 12,660, GMFγ KD= 16,962) colocalized with N-WASP (pY256) spots (Control shRNA= 10,879, GMFγ KD= 14,640) from 10 individual cells. Student's T-test was utilized with p-value significance at *p<0.05.

Figure 3: Phosphorylation at Y104 regulates focal adhesion clustering and GMFγ distribution. **(A)** GMFγ knockdown cells were transfected with either WT, Y104F, or Y104D-GMFγ GFP-tagged plasmids then fixed and immunostained for zyxin and vinculin. Arrowheads point to focal adhesions. **(B-E)** Imaris 9.1.2 software was used to render GMFγ (WT= 49,304, Y104F= 45,524, Y104D= 27,178) spots, zyxin (WT= 2,228, Y104F= 3,390, Y104D= 755), and vinculin (WT= 4,482, Y104F= 7,751, Y104D= 3,800) surfaces from 10 individual cells in order to quantitate number and area of surfaces (Fig. S3 and Methods). **(F,G)** Imaris 9.1.2 software was used to mask zyxin and vinculin surfaces followed by distance transformation algorithm to determine the percent of GMFγ inside or outside focal adhesions. Distance transformation creates concentric circles around object to measure distance based off the fluorescent intensity from other

AJRCMB Articles in Press. Published on 27-February-2019 as 10.1165/rcmb.2018-0352OC

objects denoted by distance scale (Methods). **(H)** Masked zyxin and vinculin channels were used to separate GMFγ localization within focal adhesions, nascent adhesions contain only vinculin, whereas mature adhesions contain both vinculin and zyxin. A one-way ANOVA was utilized for statistical analysis with a Tukey's post hoc test to compare between groups, p-value significance was set at *p<0.05, #p<0.05, ‡p<0.05.

Figure 4: Actin architecture is regulated by GMFγ phosphorylation at Y104. **(A)** GMFγ knockdown cells were transfected with WT, Y104F, or Y104D-GMFγ and LifeAct-RFP (pseudo-colored cyan) plasmids, fixed and immunostained for vinculin. Images were taken using Zeiss LSM880 confocal with Fast Airyscan module, white scale bar = 5μm, merged inset =2μm from n=10 individual cells per expression plasmid. Arrowheads point to actin fibers and focal adhesions. **(B-D)** Imaris software with Filament Tracer package was utilized to trace actin fibers and analyze actin fibers contacting vinculin, as well as branch and aster morphology (*Methods*). Rendered vinculin (WT= 1,518, Y104F= 1,137, Y104D= 780) surfaces are in magenta, actin fibers (WT= 40,070, Y104F= 29,600, Y104D= 31,064) are in cyan, while "actin asters" or beginning points are labeled yellow. A one-way ANOVA with a Tukey's post hoc test to compare between groups was utilized for statistical analysis, p-value significance was *p<0.05.

Figure 5: Myosin activation regulates the recruitment of GMFγ to focal adhesions. **(A)** GMFγ knockdown cells were transfected with WT, Y104F, or Y104D-GMFγ plasmids overnight. Cells were then trypsinized and re-plated onto collagen-I coated coverslips for 2hrs. After 2hrs cells were then treated with 20uM blebbistatin for 15 minutes then fixed, immunostained for vinculin, white scale bar = 10um. Arrowheads point to focal adhesions. **(B,C)** Imaris 9.1.2 software was utilized to render vinculin (WT=1,119, Y104F=1,801, Y104D=1,827) surfaces and GMFγ spots (WT=14,916, Y104F=14,475, Y104D=10,723) for quantification of vinculin area and percent GMFγ spots contacting vinculin surfaces. Student's T-test was utilized for statistical analysis comparing no treatment to blebbistatin for each individual mutant GMFγ (n= 10 cells). Significance was identified by *p<0.05. **(D)** HASMCs were grown to confluence in 60mm cell-culture treated dishes then subjected to 20uM (-/-) Blebbistatin treatment for 15 minutes. Cells were harvested using 1x SDS sample buffer containing 1x Protease and Phosphatase inhibitor, scraped, and boiled for 5mins. Samples were run on SDS PAGE, then electro-transferred onto nitrocellulose paper and immunoblotted for c-Abl tyr-412, total c-Abl, GAPDH, p-MLC, MLC, GMFγ tyr-104, and total GMFγ. Western Blots from n=4 individual experiments were imaged using the GE Amersham 600 and analyzed using IQTL software. **(E)** Quantification of phospho/total protein ratio normalized to GAPDH was graphed. Student's T-test was used to compare the effect of blebbistatin treatment with significance indicated by *p<0.05.

Figure 6: Phosphorylated GMFγ is upregulated in asthmatic HASMCs and contributes to its enhanced migratory phenotype. **(A)** Normal HASMC and airway smooth muscle cells isolated from 5 different asthmatic donors were grown to confluence in 60mm cell-culture treated dishes, then harvested with 1x SDS sample buffer containing 1x Protease and Phosphatase inhibitor, scraped and boiled for 5 mins. Samples were run on SDS PAGE, then electro-transferred onto nitrocellulose paper and immunoblotted for phospho-GMFγ (custom antibody Methods), Total GMFγ, and GAPDH. Western Blots were imaged using the GE Amersham 600 and analyzed using IQTL software. **(B)** Quantification of phospho/total protein ratio normalized to

GAPDH was graphed. Student's T-test was used to compare Normal vs. Asthma GMFγ expression with significance indicated by *p<0.05. **(C-E)** Cells were serum-starved overnight then re-plated onto collagen-I coated 6-well dishes in 10% FBS medium. Time-lapse microscopy was utilized to track NHASMC and asthmatic HASMC migration with a start time after 2hrs post-seeding. Images were taken every 10 minutes for 16hrs. Migration plots were generated using an ImageJ plugin to trace individual cells migratory pattern. **(F,G)** Graphical comparisons represent the calculated speed and accumulated distance for each cell type. Two-tailed one-way ANOVA with Tukey's post hoc test was used (*p<0.05, NHASMC n=45, asthmatic HASMC n=57, Y104F-GMFγ expressing asthmatic HASMC n=49, n = pooled cell numbers from 4 non-asthmatic human donors and 5 asthmatic human donors).

Figure 7: Model: Phosphorylation state of GMFγ dictates its localization and functionality to regulate cell migration. **(1a)** At the leading edge, cellular cues trigger the enrichment of phosphorylated GMFγ. **(1b)** There, phospho-GMFγ recruits N-WASP (pY256) to the leading edge to enhance actin re-organization through Arp2/3 activation. **(1c)** Increased actin remodeling leads to increased protrusion extension and enhances lamellipodial dynamics. **(2a)** Upon myosin activation, non-phosphorylated GMFγ becomes enriched within focal adhesions, which includes talin and integrins, as well as many other proteins . **(2b)** Non-phosphorylated GMFγ recruits N-WASP (pY256) and increases linear actin formation and focal adhesion assembly. **(2c)** Non-phosphorylated GMFγ promotes actin re-organization, focal adhesion clustering and recruitment of zyxin to enhance focal adhesion maturation. Sustained mechanical tension will increase c-Abl activation within focal adhesions leading to phosphorylation of GMFγ, thus liberating it from Arp2/3 and returning GMFγ to the leading edge.

AJRCMB Articles in Press. Published on 27-February-2019 as 10.1165/rcmb.2018-0352OC

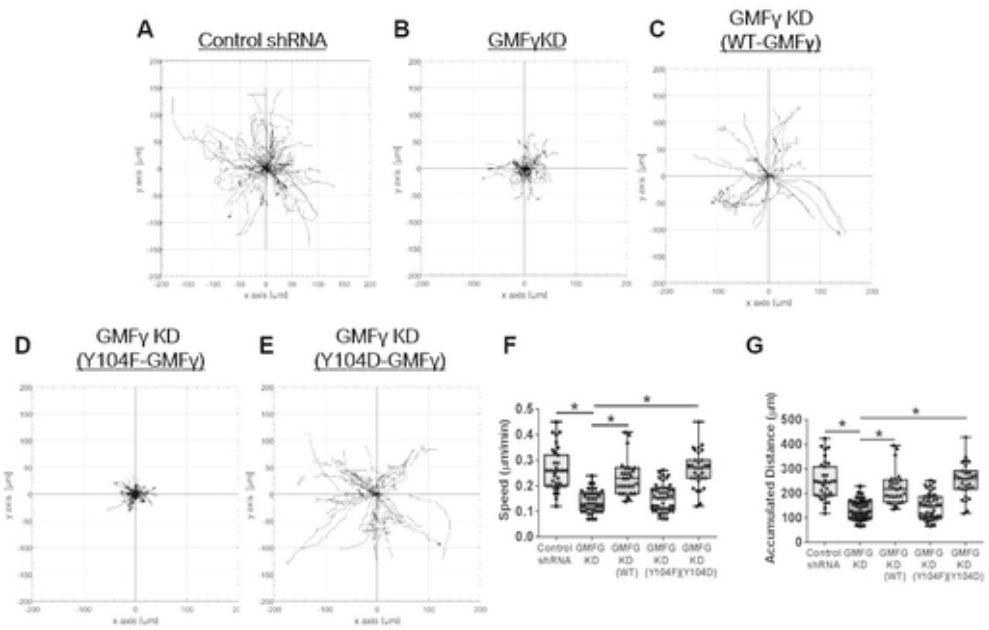

Figure 1

43x28mm (300 x 300 DPI)

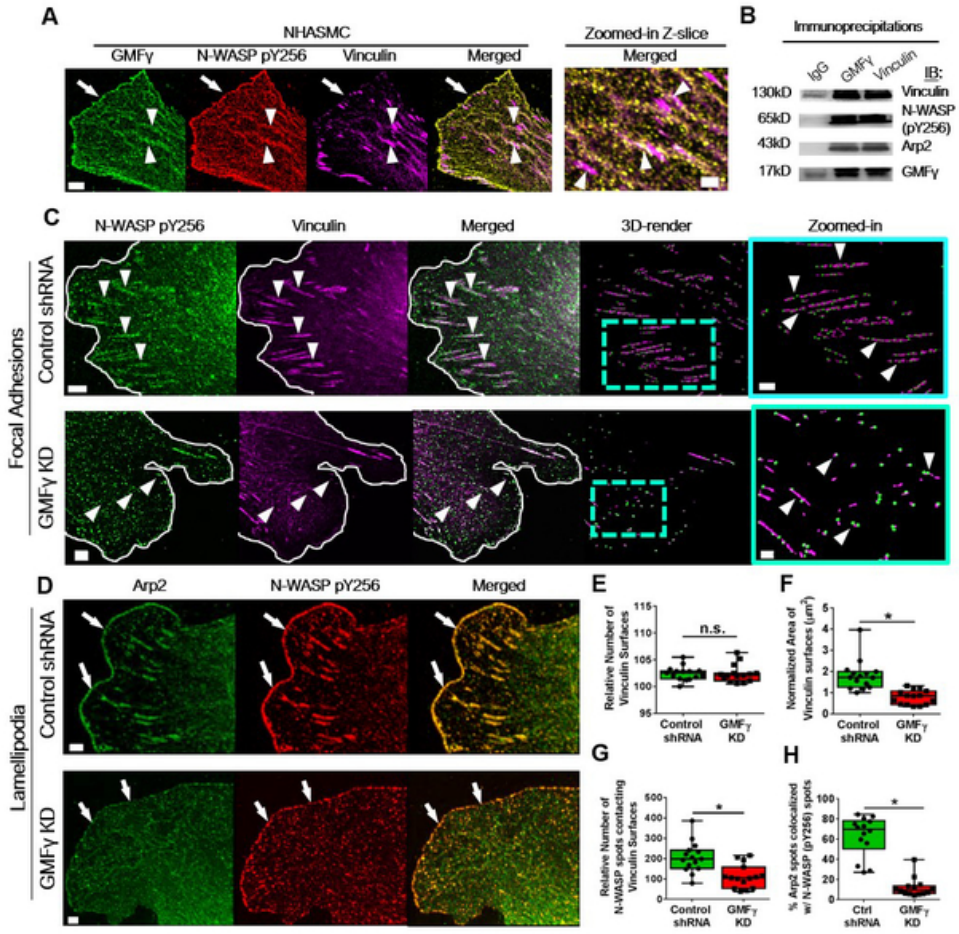

Figure 2

26x25mm (600 x 600 DPI)

AJRCMB Articles in Press. Published on 27-February-2019 as 10.1165/rcmb.2018-0352OC

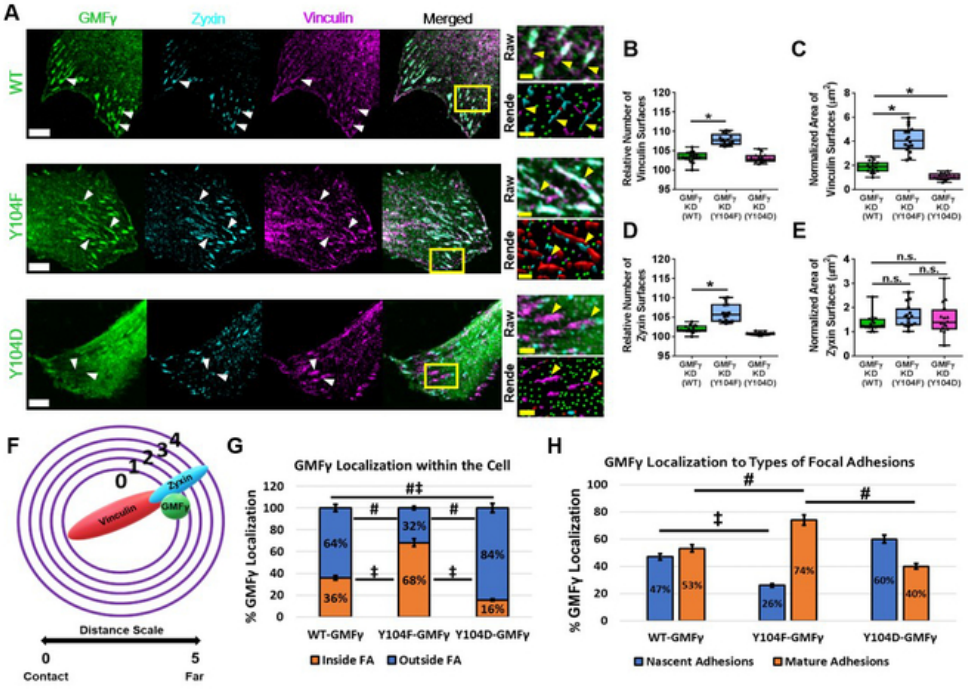

Figure 3

28x20mm (600 x 600 DPI)

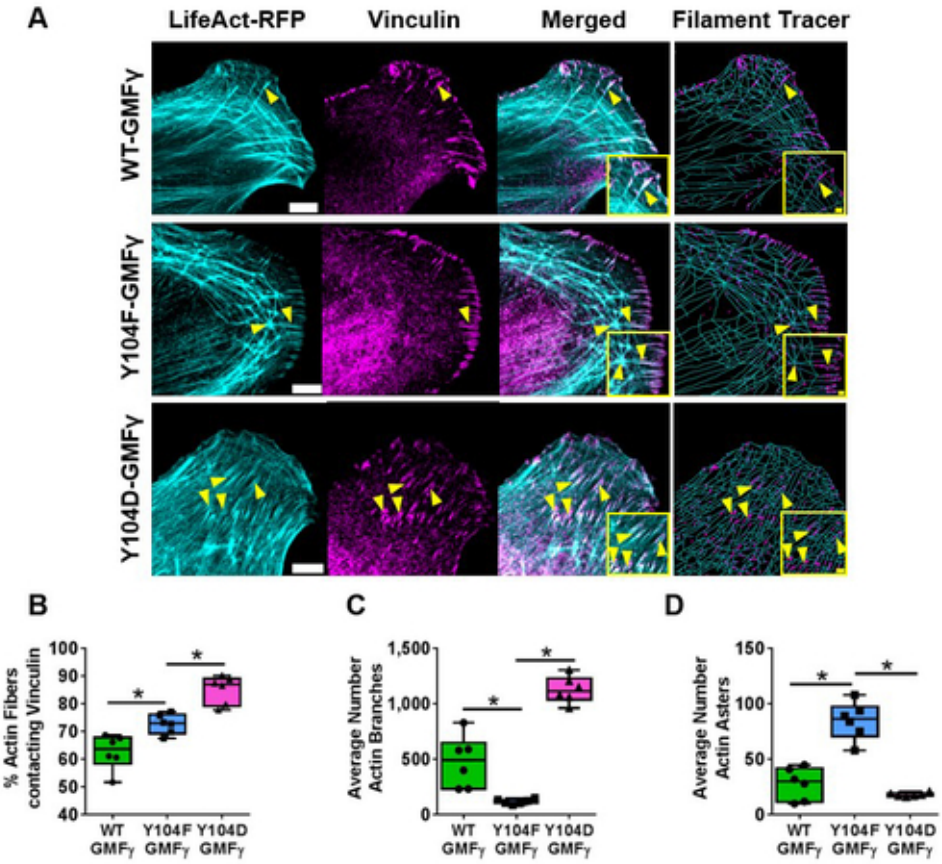

Figure 4

22x19mm (600 x 600 DPI)

AJRCMB Articles in Press. Published on 27-February-2019 as 10.1165/rcmb.2018-0352OC

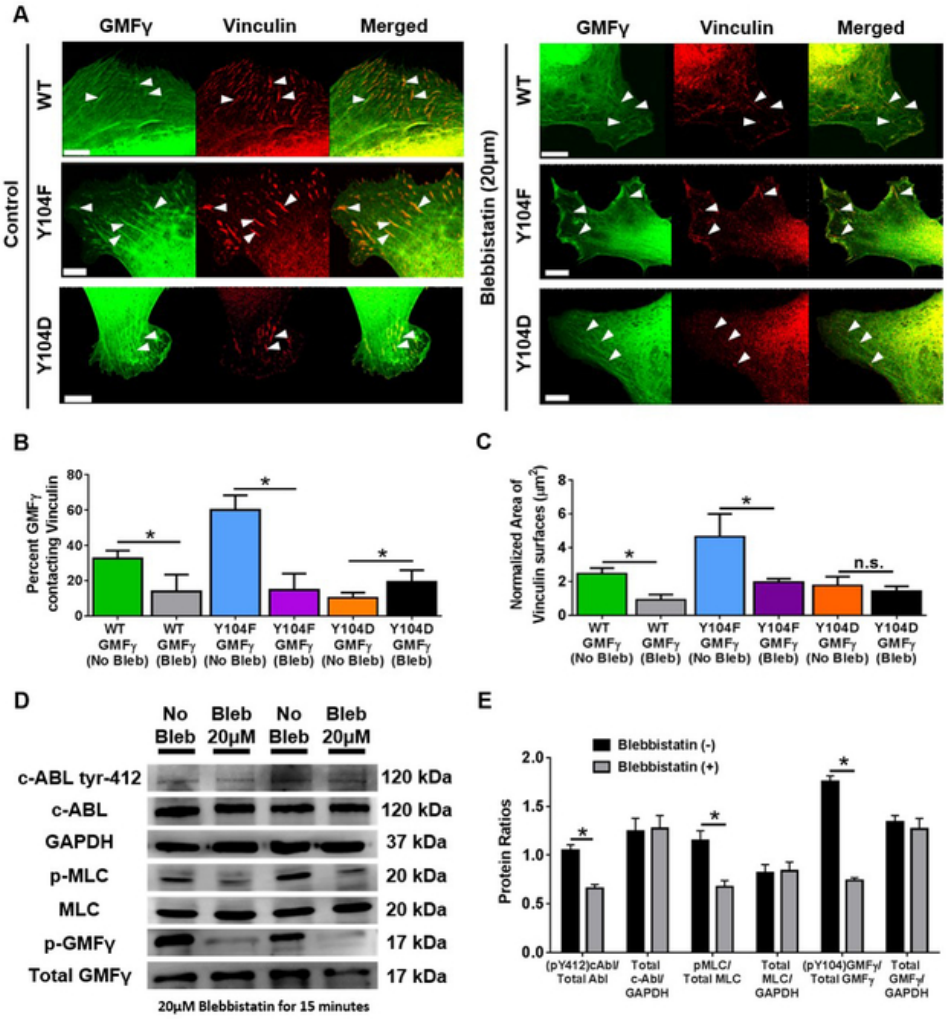

Figure 5

27x28mm (600 x 600 DPI)

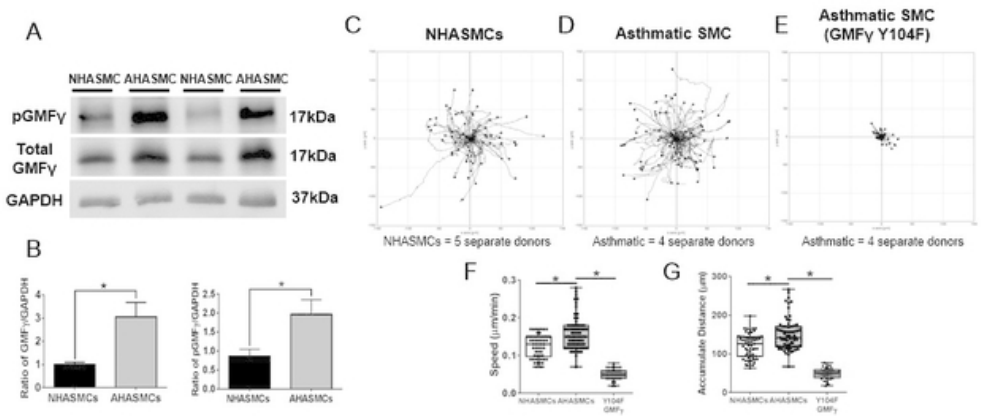

Figure 6

26x11mm (600 x 600 DPI)

AJRCMB Articles in Press. Published on 27-February-2019 as 10.1165/rcmb.2018-0352OC

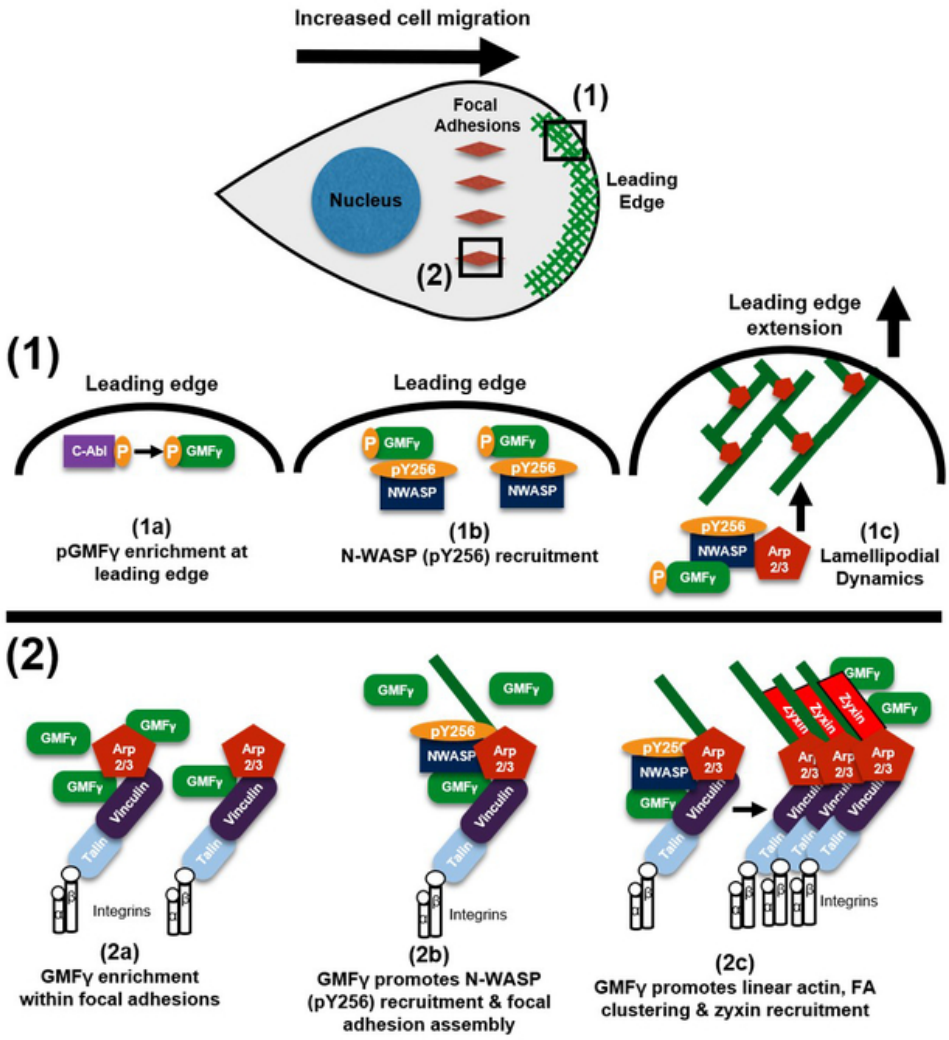

Figure 7

27x28mm (600 x 600 DPI)

EXTENDED SUPPLEMENTAL METHODS

Cell Culture

Human airway smooth muscle cells (HASMCs) were prepared from bronchi and adjacent tracheas of control subjects (died from non-asthmatic causes) obtained from the International Institute for Advanced Medicine (50). Non-asthmatic and asthmatic human airway smooth muscle cells were also obtained from Dr. Reynold A. Panettieri of Rutgers University (29, 33). Human tissues were non-transplantable and consented for research. This study was approved by the Albany Medical College Committee on Research Involving Human Subjects. Briefly, muscle tissues were incubated for 20 min with dissociation solution [130 mM NaCl, 5 mM KCl, 1.0 mM $CaCl_2$, 1.0 mM $MgCl_2$, 10 mM Hepes, 0.25 mM EDTA, 10 mM D-glucose, 10 mM taurine, pH 7, 4.5 mg collagenase (type I), 10 mg papain (type IV), 1 mg/ml BSA and 1 mM dithiothreitol]. All enzymes were purchased from Sigma-Aldrich. The tissues were then washed with Hepes-buffered saline solution (composition in mM: 10 Hepes, 130 NaCl, 5 KCl, 10 glucose, 1 $CaCl_2$, 1 $MgCl_2$, 0.25 EDTA, 10 taurine, pH 7). The cell suspension was mixed with Ham's F12 medium (ThermoFisher) supplemented with 10% (v/v) fetal bovine serum (FBS) and antibiotics (100 units/ml penicillin, 100 µg/ml streptomycin). Cells were cultured at 37°C in the presence of 5% CO_2 in the same medium. The medium was changed every 3–4 days until cells reached confluence, and confluent cells were passaged with trypsin/EDTA solution. Cell lines from five control subjects were available for the experiments. In some cases, duplicated experiments were performed for a cell line from a donor. For immunostaining experiments, cells were plated at 8,000 cells/ml onto collagen I coated coverslips (10 µg/ml) for 60 minutes. All live-cell experiments were performed using

AJRCMB Articles in Press. Published on 27-February-2019 as 10.1165/rcmb.2018-0352OC

phenol-red free DMEM/F12 with 20mM HEPES, 4mM L-glutamine and contained 10% FBS on 35mm No. 0 collagen I coated glass bottom dishes (MatTek).

Reagents and Transfection

mTagRFP-T-Lifeact-7 (Addgene plasmid # 54586) was a gift from Michael Davidson (Florida State University, Tallahassee, FL). Human GMFγ DNA (NCBI Accession Number, NM_004877.2) was synthesized by Life Technologies and subcloned into bacterial vectors pEGFP. Quickchange II site-directed mutagenesis kit (Agilent Technologies, Santa Clara, CA) was used to generate Y104F mutant (phenylalanine substitution at Tyr-104). The 5'-primer was 5'-GCC GGA ACA ACA GAT GAT GTT CGC AGG GAG TAA AAA CAG G-3'. The 3'-primer was 5'-CCT GTT TTT ACT CCC TGC GAA CAT CAT CTG TTG TTC CGG C-3'. To generate Y104D mutant (aspartic acid substitution at Tyr-104). The 5'-primer was 5'-GCC GGA ACA ACA GAT GAT GGA TGC AGG GAG TAA AAA CAG-3'. The 3'-primer was 5'-CTG TTT TTA CTC CCT GCA TCC ATC ATC TGT TGT TCC GGC-3'.

Transfections for migration assay were performed with 0.5 µg DNA using FuGene HD Transfection Reagent (Promega Corporation Madison, WI). Cells were transfected overnight, and the media was changed to 10% FBS/F12 before running the migration assay. Transfections of cells for fixed and live-cell confocal microscopy were performed with Neon electroporation and Neon reagents (ThermoFisher MPK10025) with pulse width/number optimized for this cell line. Cells were transfected and allowed to adhere overnight, and the media was changed to 10% FBS/F12. All transfected cell experiments were carried out 16hrs post-transfection.

Lentiviral particles containing shRNA specific for GMFγ or non-targeting control shRNA were purchased from Santa Cruz Biotechnology. HASM cells were infected with control shRNA lentivirus (Cat#sc-108080) or GMF-γ shRNA lentivirus (Cat#sc-97348-V) for 12hrs. They were then cultured for 3-4 days. Positive clones expressing shRNAs were selected by puromycin. Immunoblot analysis was used to determine the expression levels of GMF-γ in these cells. GMF-γ KD cells and cells expressing control shRNA were stable at least five passages after initial infection. In addition, our laboratory previously characterized stable c-Abl KD cells (27, 28, 30).

Primary antibodies used for immunofluorescence (IF) and western blot (WB): anti-goat total GMFγ (E-13) (1:25_IF, 1:50_WB, Santa Cruz Biotech Lot# B0915, Cat# sc-168016), anti-rabbit N-WASP Y256 (1:25_IF, 1:100_WB, EMD Millipore Lot# 2795491, 2838736, Cat# AB1966), anti-mouse Arp2 (E-12) (1:25_IF Santa Cruz Biotech Lot# B0612, Cat# sc-166103), anti-mouse vinculin (1:25_IF Invitrogen, ThermoFisher Lot# RA 2147394, Cat# MA1-34629), anti-rabbit vinculin (1:25_IF, 1:100_WB Sigma Aldrich), anti-mouse zyxin (1:25_IF Santa Cruz Biotech Lot# B1317, Cat# sc-293448). The anti-rabbit phospho-GMFγ (Tyr-104) antibody was custom made by Thermo Scientific (Pierce). The sequence of the peptide for generating phospho-GMF-γ antibody was CKPEQQMMY(P)AGSKNRLVQTA (NCBI Accession Number, NM_004877.2). Secondary antibodies were all purchased from Invitrogen (ThermoFisher), which includes Alexa 405, 488, 555, 546, and 647 at a concentration of 1:100.

Western Blot Analysis

Cells lysed with 2x SDS sample buffer composed of 1.5% dithiothreitol, 2% SDS, 80mM

AJRCMB Articles in Press. Published on 27-February-2019 as 10.1165/rcmb.2018-0352OC

Tris-HCl (pH 6.8), 10% glycerol and 0.01% bromophenol blue were boiled for 5 mins and separated onto SDS PAGE, then electro-transferred to nitrocellulose paper. Membranes were blocked using 2% bovine serum albumin (BSA) in PBS for 1hr and then probed with specific primary antibodies followed by horseradish peroxidase-conjugated secondary antibody (Fisher Scientific). Proteins were visualized with Amersham enhanced chemiluminescence (ECL) select Western Blotting Detection Reagent (GE Healthcare Lot# 9774291 Cat# 45000999PM) using the Amersham Imager 600 (GE Healthcare). The levels of total protein or phosphoprotein were quantified by scanning densitometry of immunoblots (IQTL software by GE Healthcare).

NHASMC were grown to 100% confluence in 60mm cell-culture dishes and then subjected to blebbistatin (-/-Blebbistatin Sigma Aldrich Catalog #B0560-1MG, Lot #SLBK5210V) treatment 20uM in 1ml of Serum-free Ham's F12 media for 15 minutes. After 15 minutes cells were harvested on ice and washed quickly twice with 1x PBS, then 150ul of 2x SDS sample buffer with 1x Halt Protease and Phosphatase Inhibitor single-use cocktail, EDTA free (ThermoScientific Product #78443 Lot #SJ256802) was added, cells scraped, boiled for 5 mins and separated onto SDS PAGE, then electro-transferred to nitrocellulose paper. Membranes were blocked using 2% BSA in PBS for 1hr and then probed with c-Abl tyr-412 (1:500 Santa Cruz Biotech sc-101626, Lot #K0911), total c-Abl (1:500 Santa Cruz Biotech sc-23, Lot #I2116), GAPDH (6C5) (1:4000 Santa Cruz Biotech sc-32233, Lot #K0315), pMLC (1:500 Santa Cruz Biotech sc-19849-R, Lot #B2411), MLC antibody (1:1000 custom made).

Co-Immunoprecipitation

Cells were plated in 100mm cell culture dishes and allowed to grow to 90-100% confluence. Media was changed to SFM overnight. Media was removed and Lysis buffer (10% Triton X 100, 0.5M EDTA, 1M HEPES pH 7.6, 20% SDS, 100x Halt protease/phosphatase single-use Inhibitor cocktail Cat# 78442 Lot# RH235957) was added and incubated at 4°C for 10 minutes. Cells were scraped into 1.5ml tubes and rotated for 1hr at 4°C. Centrifugation at 13.0rpm (x1000g) for 20 minutes and removal of the supernatant was placed in new 1.5ml tube. Addition of Protein A/G Plus-agarose (Santa Cruz Biotech Lot# B0116 Cat# sc-2003) rotated for 30 minutes at 4°C. Centrifuge for 5 minutes and removal of supernatant and placed in new 1.5ml tube. Subsequently, the addition of primary antibody or normal IgG as control were added to supernatant and rotated overnight at 4°C. Following incubation, Protein A/G with agarose was added and rotated for 3 hours at 4°C then centrifuged for 15 minutes at 13,000 rpm (x1000g) and removal of supernatant. Pellets were resuspended in IP Wash Buffer (5M NaCl, 1M Tris pH 7.6, 10% Triton x100, and H_2O), centrifuged and the supernatants discarded 4 times. Pellets were saved and mixed with 2x SDS buffer, then boiled for 5 minutes and spun down. Co-IP samples were loaded and separated on an SDS PAGE gel, where they were electro-transferred onto nitrocellulose paper and immunoblotted with the correct primary antibodies. Visualization of co-IP was carried out using Amersham ECL (GE Healthcare) and imaged using the Amersham Imager 600 (GE Healthcare).

Immunofluorescence Microscopy

Cells were plated onto collagen I coated coverslips for 60mins, then fixed using 4% paraformaldehyde for 15minutes at room temperature and then permeabilized with 0.2% Triton X 100 in PBS. Coverslips were washed 3x for 5minutes with 1x PBS in between

AJRCMB Articles in Press. Published on 27-February-2019 as 10.1165/rcmb.2018-0352OC

each step. Coverslips were blocked using 2% BSA/PBST for 30minutes then primary antibodies were added with 2% BSA/PBST and incubated for 1hr each. Secondary antibodies were added at a concentration of 1:200 for 1hr each. Coverslips were fixed onto slides using Prolong Diamond mounting medium (ThermoFisher).

Imaging for fixed-cells and live-cells was conducted on a Zeiss LSM 880 NLO confocal microscope with Fast Airyscan module (Carl Zeiss Microscopy Jena, Germany) equipped with 63x oil 1.4 numerical aperture (NA) objective lens and collected through a 32-channel GaAsP detector as 0.2 Airy units per channel (Huff, J. 2016). Cells were imaged using Argon405 (488 nm) laser and BP 420-480/BP 495-620 filter for GFP; DPSS 561-10 (561 nm) laser and BP 495-550/LP 570 filter for RFP, and HeNe633 (633nm) laser and BP 570-620/LP 645 filter for far-red. Z-stack collecting was under Nyquist sampling and with the fast airyscan SR settings. Z-stacks were acquired at an average of 11 slices with 0.17μm distance between each slice. Live-cell imaging of GMFγ-GFP tagged mutants, Life-Act-RFP, and paxillin-mcherry constructs utilized the Fast-Airyscan module on the Zeiss LSM 880 confocal microscope. Z-stack live-images were taken at an average of 6 slices with 0.17μm distance between slices for 10 or 20 minutes at a frame rate of 10 seconds. Microscope software used is the Zen Black 2 edition to process images for the Airyscan. The microscope has an incubation chamber set to 30-37°C and has 5% CO_2 for live-cell imaging. Time-lapse microscopy was achieved by using a Leica A600 microscope with a 6-well incubator chamber hooked up to 5% CO_2. Epifluorescence imaging was utilized for cells that were transfected with fluorescent protein constructs. Only cells expressing specific GFP fluorescent constructs were imaged and used for analysis. Epifluorescence was achieved by using a GFP filter cube. Multi-position marking

function was used to designate specific x and y coordinates for the time-lapse capture of images every 10 minutes for a 16-hour experimental period.

Image Analysis

Spots to Surfaces Analysis

Imaris 9.1.2 (Bitplane, Oxford Instruments) software was used to generate and analyze the distance between spots and surfaces using a distance transformation. The surface module uses an algorithm to create 3D-reconstructed objects based upon fluorescent intensity, quality of rendering, and then a threshold was applied for focal adhesion areas ≥ 0.5μm. Once surfaces were created, MatLab algorithms were used to measure the total number and area of each surface. If the image contained two surfaces (vinculin and zyxin), a mask of each surface was created. Any voxel outside of the masked surface is signified as having an intensity value greater than 0.00. This allows separation of channels inside regions within a masked surface that is contacting both vinculin and zyxin or just vinculin alone. A separate algorithm was used to create spots based upon the fluorescent intensity and quality for either GMFγ or N-WASP pY256 channels. Once spots were created, a plugin was used to measure the total number of spots for specific channels. Also, a separate plugin was used to threshold on spots closest to surfaces another form of distance transformation (Figure 4F). From there a percentage of the number of spots closest to surface to a total number of spots could be generated for analysis (See Figures S2 and S3).

Focal Adhesion Dynamics Analysis

AJRCMB Articles in Press. Published on 27-February-2019 as 10.1165/rcmb.2018-0352OC

Imaris 9.1.2 (Bitplane, Oxford Instruments) software was used to generate and analyze Paxillin 3D-rendered surfaces over time. Paxillin surfaces were rendered based on fluorescent intensity, quality, and area. A Brownian algorithm was utilized to track the movement of paxillin surfaces over time. Paxillin surfaces were filtered based on an area >1um and track duration (minimum of 300seconds). Each paxillin surface was individually checked in vantage plot module to make sure the rendering was accurate over the entire time course. All paxillin surfaces were input into a vantage plot for each individual cell and analyzed for time changes in the area, bounding box length, intensity fluorescent sum, and volume. Vantage plots were saved as Microsoft Excel spreadsheets (Microsoft Office 365 package). Spreadsheets were sorted and filtered by Time and TrackID. Graphs of individual paxillin surfaces were created based off area over time (300second duration). Each cell (n=10 cells per WT, Y104F, Y104D-GMFγ) contained an average of 250 individual paxillin surfaces that were selected based on threshold criteria and were individually graphed. Representative cells with 2 paxillin ROI's per GMFγ expression were presented in the main text.

Filament Tracer Analysis

Imaris 9.1.2 (Bitplane, Oxford Instruments) software was used to generate and analyze actin fiber organization. Filament Tracer has been utilized to characterize neuron and dendrite morphology. Here we adapted this software package to analyze the actin cytoskeleton morphology and percent actin fibers contacting vinculin. Actin fibers were rendered using fluorescent intensity, the diameter of the largest fiber and quality. Vinculin objects were rendered using the surface module based on fluorescent intensity, surface area equivalent to >1μm, and quality. A mask was applied to the rendered actin fibers

and a new channel was created. Next a new surface module was used to render the masked channel of actin fibers. MatLab plugin “surface-surface colocalization” was applied to vinculin and actin fiber surfaces. This plugin performs a distance transformation algorithm to identify contacting objects rendered as surfaces. A surface contacting another surface has an output of 0.00, whereas a surface not contacting another surface has an output of >1.00 based on proximity. Next statistics were performed to identify the percent actin fibers contacting vinculin surfaces: (number of surfaces with an output of 0.00)/ (total number of surfaces) for each treatment (n=6 cells per WT, Y104F, Y104D-GMFγ).

Asters were identified by fluorescent intensity and having at least 5 actin fibers radially-projecting from the center of the aster and were marked as beginning points. Actin fibers that were branching in morphology were identified by having <5 branch points per fiber. Rendered actin fibers are shown in cyan and beginning points “actin asters” are shown in yellow. Imaris software “Filament Statistics” was applied to the rendered actin fibers and beginning point “asters” and branch points were graphed (n=6 cells per WT, Y104F, Y104D-GMFγ).

Protrusion/Retraction Analysis

The ImageJ plugin ADAPT (automated detection and analysis of protrusions), which utilizes the fluorescent intensities at the cell border to measure changes in protrusion/retraction position and velocity over time, was used to analyze Zeiss LSM 880 confocal live-cell movies (44). The input of the spatial resolution, frames per minute, thresholding method (Triangle), smoothing filter radius, erosion iterations, spatial filter

AJRCMB Articles in Press. Published on 27-February-2019 as 10.1165/rcmb.2018-0352OC

radius, temporal filter radius, cortex depth, visualization line thickness, and minimum/maximum velocity parameters will generate protrusion boundaries based on changes in fluorescence intensity. Output analysis generates values of protrusion trajectory, protrusion/retraction velocity, and protrusion/retraction events.

Statistical Analysis

All data were analyzed using GraphPad Prism version 6.00 software (Windows, GraphPad Software, La Jolla, CA). A two-tailed one-way ANOVA followed by Tukey's multiple comparisons test was used for comparing Time-lapse microscopy parameters, lamellipodial protrusion/retraction velocity and events, comparing vinculin and zyxin area and number, all filament tracer experiments, and comparing the percent of GMFγ inside or outside adhesions (significance was determined by a $p<0.05$). A two-tailed Student's T-test was used to determine a significance of $p<0.05$ for knockdown cell focal adhesion parameters, protein level expression, and "wound" closure rates. A two-tailed Student's T-test was used to determine a significance of $p<0.05$ for blebbistatin-treated cells. Number of independent experiments is indicated within figure legends. Box and whisker plots and bar graphs were used to represent data shown.

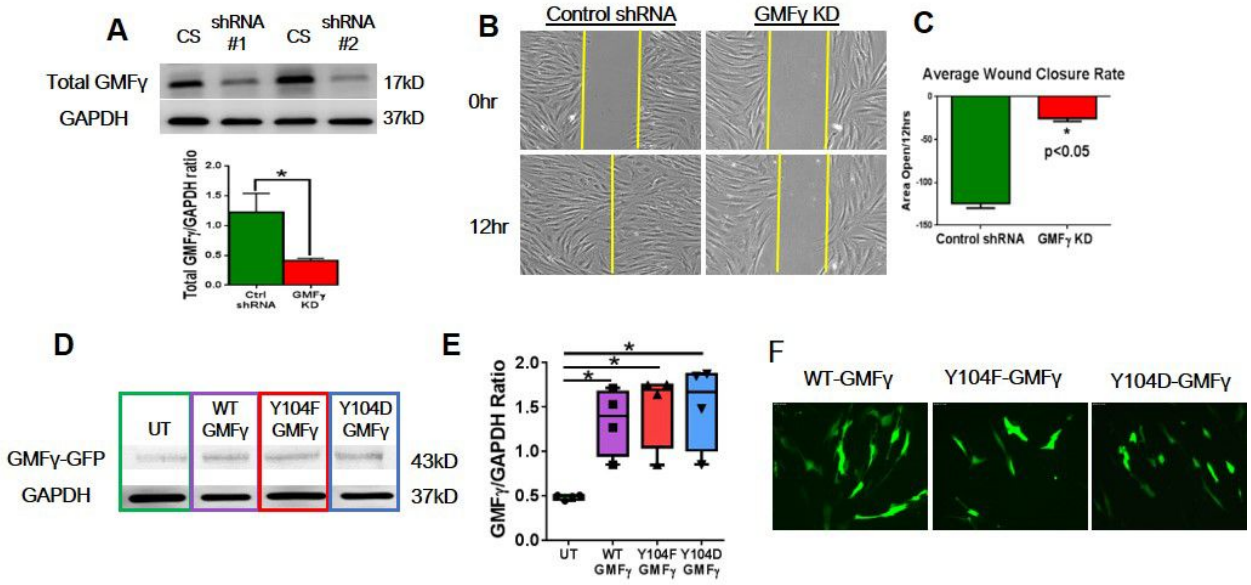

Figure S1: Knockdown of GMFγ inhibits directional migration. (A) NHASMC were infected with Control shRNA lentiviral particles or two separate pools of GMFγ shRNA lentiviral particles. Cells were selected using Puromycin over the course of 7 days post infection. Cells were harvested with 1x SDS buffer and ran on SDS-PAGE gel then electro-transferred onto nitrocellulose paper and immunoblotted for GMFγ and GAPDH to confirm successful knockdown n=4 independent experiments. **(B)** Stable-selected knockdown cells or control shRNA expressing cells were plated on collagen I coated 6-well dishes and grown to confluence. Once confluent each 6-well dish was scratched with a 1µl pipette tip and multi-positions were collected immediately on a Leica A600 microscope equipped with 5% CO_2 and 37°C incubation chamber. Images were collected every 10 minutes over the course of 12hrs. Images shown are beginning and end-points at time 0 and 12hrs post-scratch. Yellow lines outline the border of cells. N=12 independent experiments. **(C)** Quantification of the area between the scratch over the 12hr time-course was completed using NIH ImageJ software. Student's T-test was used to compare Control shRNA to GMFγ shRNA expressing cells, significance was *p<0.05 from n=12 independent experiments. **(D)** GMFγ shRNA expressing cells were transfected with 0.5µg eGFP-tagged WT, Y104F-, Y104D-GMFγ plasmids using FuGene HD Transfection Reagent. After 16hrs post-transfection, cells were harvested for Western Blot. Nitrocellulose paper was immunoblotted for GMFγ and GAPDH and imaged using an Amersham 600 imager. N=4 independent experiments. **(E)** The levels of total protein were quantified by scanning densitometry of immunoblots (IQTL software by GE Healthcare), One-way ANOVA with Tukey's posthoc test was used to determine significance at *p<0.05 from n=4 independent experiments. **(F)** Epifluorescent imaging of GFP-expressing WT, Y104F-, Y104D-GMFγ knockdown cells. Images were taken at 10x using a Leica A600 microscope from n=4 independent experiments.

AJRCMB Articles in Press. Published on 27-February-2019 as 10.1165/rcmb.2018-0352OC

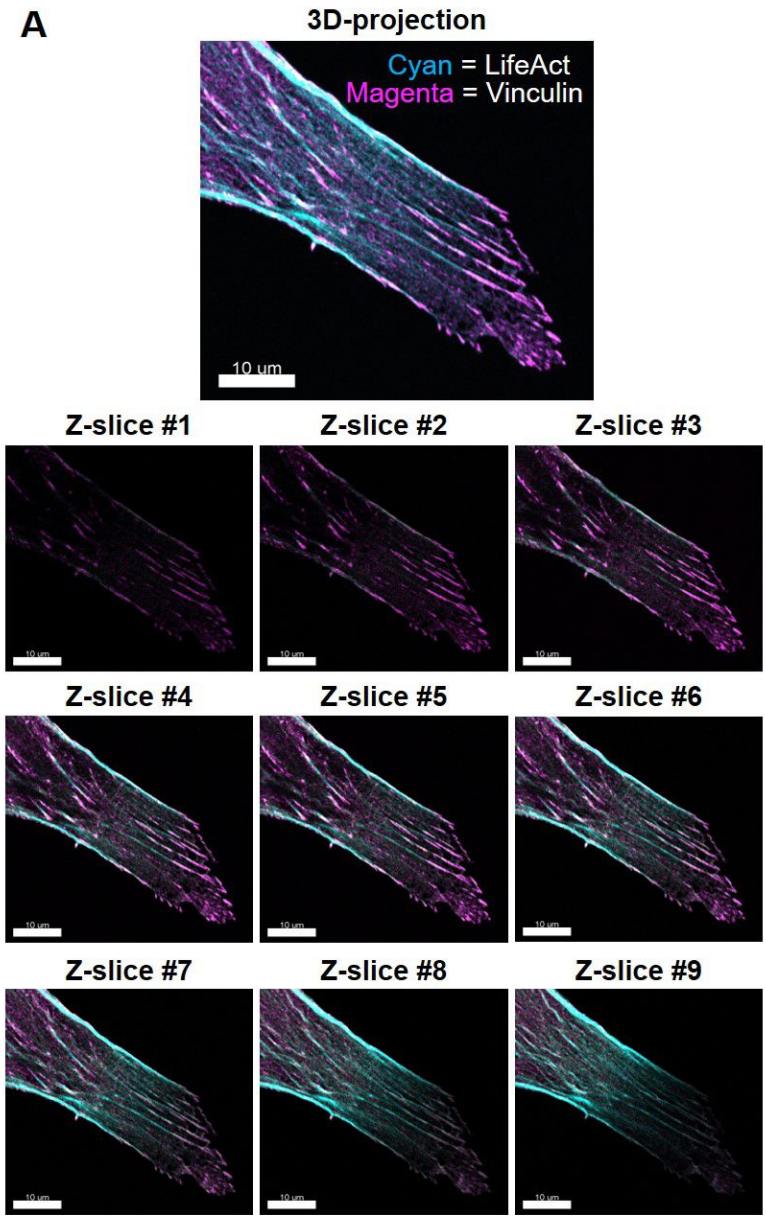

Figure S2: Focal adhesions within Human airway smooth muscle cells span multiple Airyscan confocal z-slices. (A). Human airway smooth muscles cells electroporated with LifeAct-RFP plasmid were then directly plated onto collagen-I coated glass MatTek dishes and allowed to adhere overnight. Following day cells were fixed with 4% PFA and immunostained for Vinculin. Images were taken on a Zeiss LSM 880 confocal with Fast Airyscan module. N=20 individual cells. Imaris software pseudo-colored the LifeAct-RFP channel to cyan for visualization purposes only. Note how vinculin-associated focal adhesions span multiple z-slices in human airway smooth muscle cells.

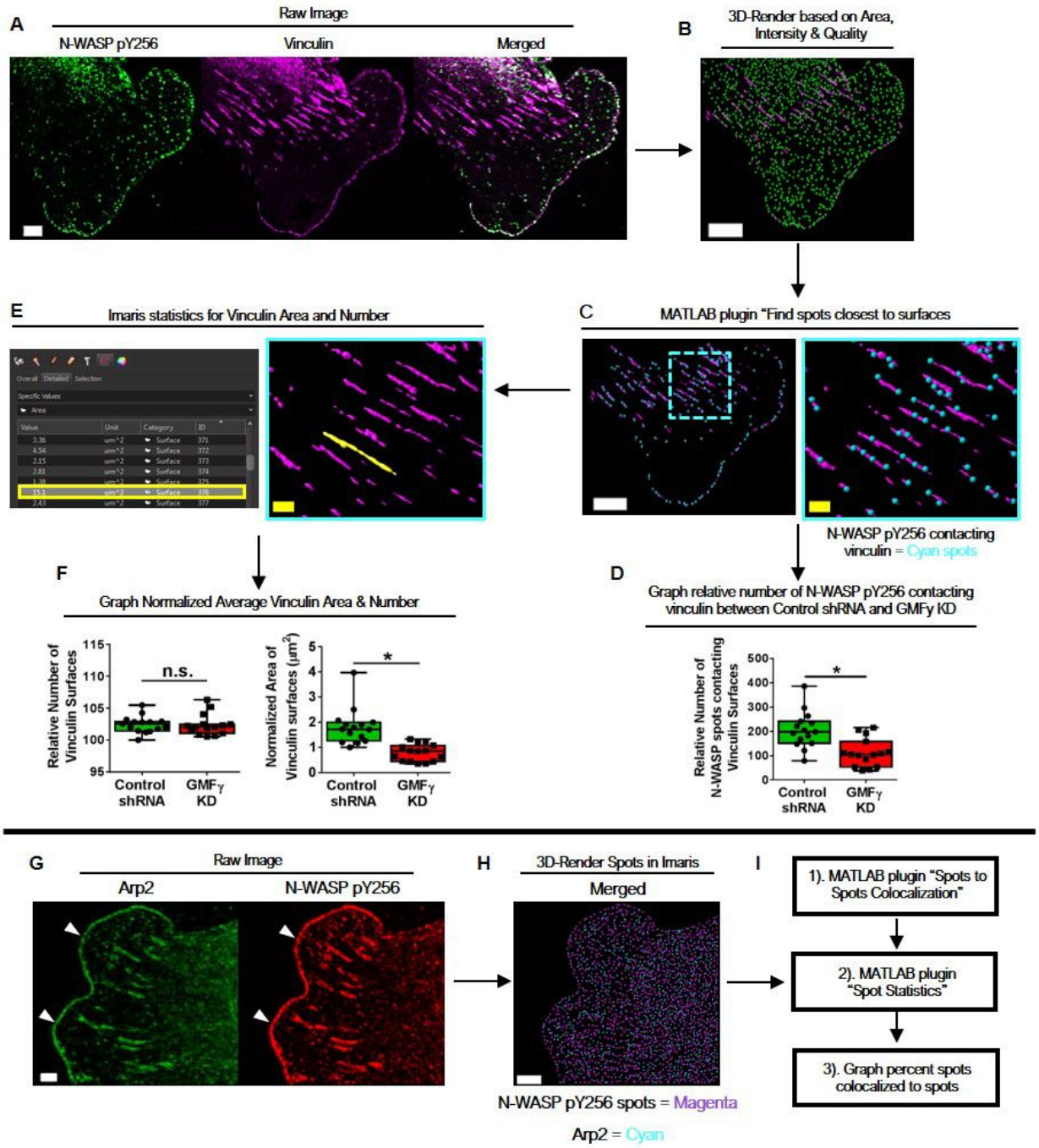

AJRCMB Articles in Press. Published on 27-February-2019 as 10.1165/rcmb.2018-0352OC

Figure S3: Imaris image analysis protocol for knockdown of GMFγ and its effects on focal adhesion dimension and N-WASP localization. (A) Raw 3D-projection immunofluorescent image taken using Fast Airyscan module on a Zeiss LSM880 confocal microscope. **(B)** Input image into Imaris software. Utilize surface module to 3D-reconstruct vinculin into surfaces based on fluorescent intensity, area, and quality. Utilize spot module to 3D-reconstruct punctate N-WASP (pY256) into spots based on fluorescent intensity, number of voxels, and quality. **(C)** MatLab plugin "Find spots close to surfaces" utilizes a distance transformation algorithm to identify objects based on their proximity in 3D-orientation. An output of 0.00 means the objects are contacting and any object >0 is not contacting any objects. **(D)** A relative number of objects contacting a surface can be generated based on this distance transformation. **(E)** Any 3D-reconstructed surface will have multiple statistics associated with itself. For example, the yellow highlighted surface has a surface area of 15μm^2 and an object ID of 376. **(F)** Using the Imaris statistics an average area and number of vinculin surfaces can be graphed. **(G)** Arp2 and N-WASP (pY256) were immunostained and imaged using the Fast Airyscan module on a Zeiss LSM880 confocal microscope. **(H)** Imaris software was used to 3D-reconstruct Arp2 and N-WASP (pY256) spots using fluorescent intensity, number of voxels, and quality filters. **(i)** MatLab plugin "Spots to Spots Colocalization" was used to determine how many Arp2 and N-WASP (pY256) spots were colocalized based on the distance transformation. N=10 individual cells.

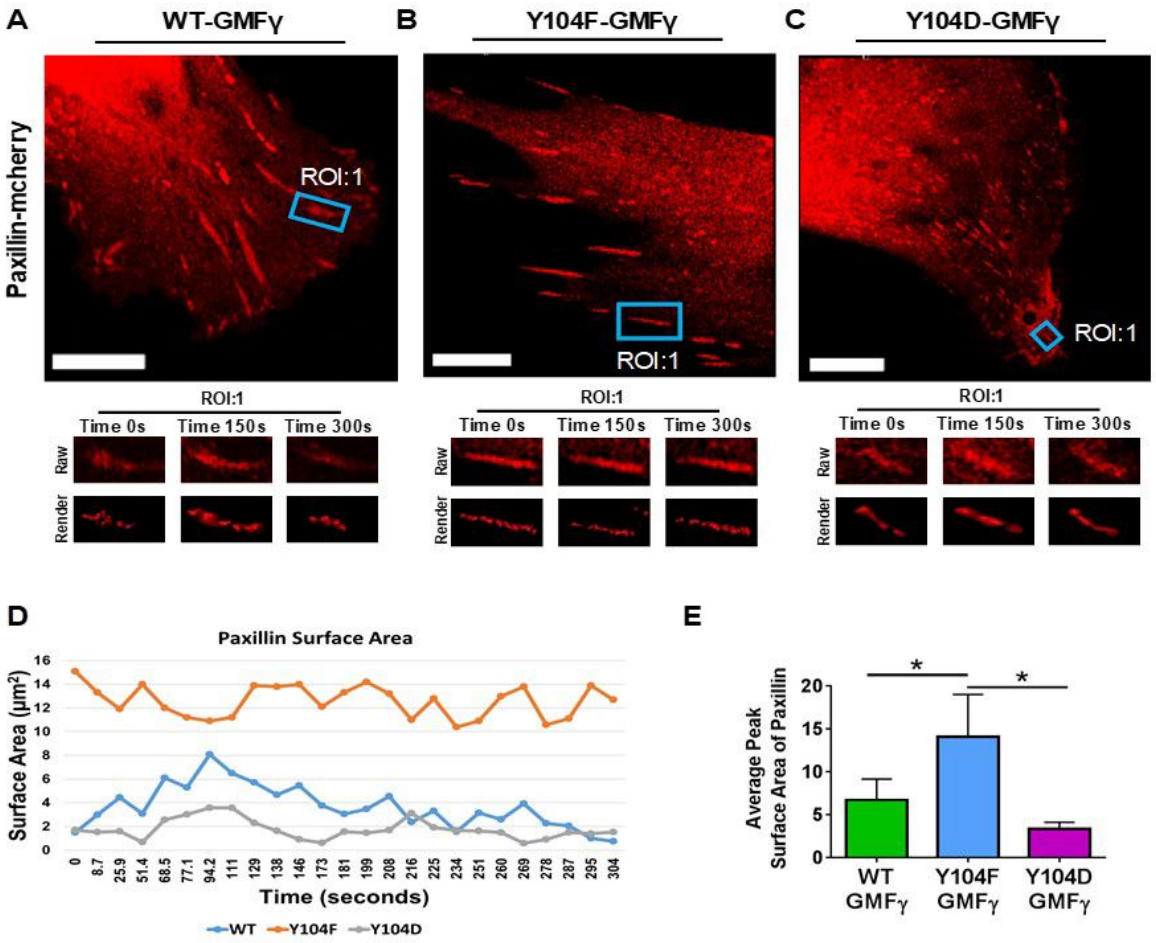

Figure S4: GMFγ phosphorylation at Y104 impacts focal adhesion dynamics in live cells. (A-C) GMFγ knockdown cells were transfected with WT, Y104F, or Y104D-GMFγ and paxillin-mcherry plasmids. Imaris 9.1.2 software was utilized to render paxillin surfaces based on fluorescent intensity, quality, area, and track duration (threshold minimum of 300 seconds). Brownian motion algorithm was used to track changes in the area over time (*Methods*). Representative paxillin regions of interest (ROI's) were selected and shown as raw or rendered images over 300secs (Rendered Paxillin: WT- GMFγ n=1,489, Y104F-GMFγ n=2,012, Y104D-GMFγ n=2,387) from n=10 individual cells per expression plasmid.**(D)** Line graphs represent the changes in paxillin area during track duration. **(E)** Graph of the average peak surface area for each reconstructed paxillin. One-way ANOVA with Tukey's posthoc test, significance *p<0.05.

AJRCMB Articles in Press. Published on 27-February-2019 as 10.1165/rcmb.2018-0352OC

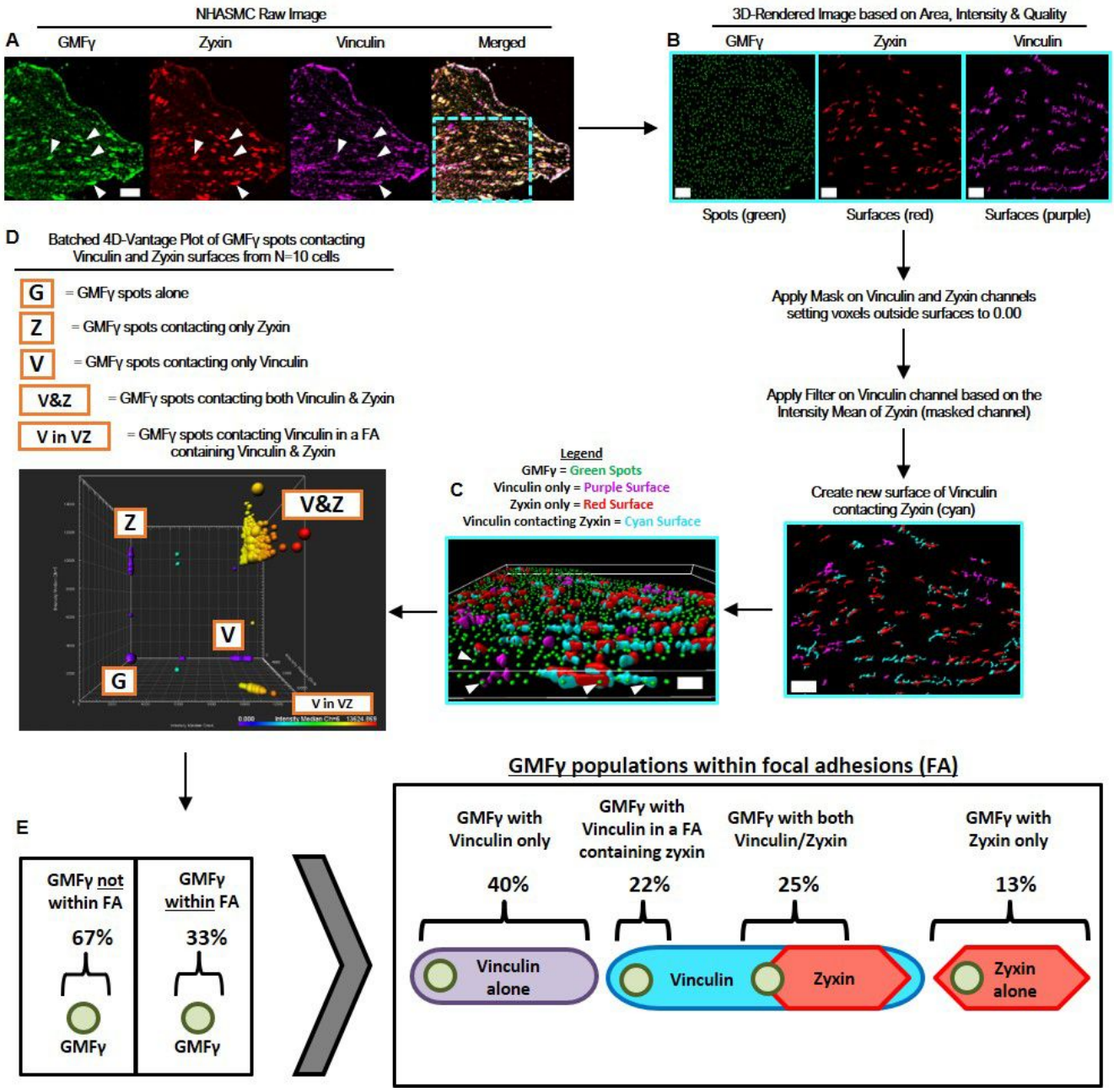

Figure S5: Imaris image analysis protocol for GMFγ mutant expression and its effects on focal adhesion dimension and GMFγ localization. (A) Raw 3D-projection immunofluorescent image taken using Fast Airyscan module on a Zeiss LSM880 confocal microscope. **(B)** Input image into Imaris software. Utilize surface module to 3D-reconstruct zyxin and vinculin into surfaces based on fluorescent intensity, area, and quality. Utilize spot module to 3D-reconstruct punctate GMFγ into spots based on fluorescent intensity, number of voxels, and quality. Apply a mask on vinculin and zyxin channels setting voxels outside surfaces to 0.00. Apply filter on vinculin channel based on the fluorescent intensity mean of zyxin (masked channel). Create new surface of vinculin contacting zyxin surfaces (cyan). **(C)** Representative image displaying GMFγ spots (green), vinculin only (purple), zyxin only (red), and vinculin surfaces contacting zyxin surfaces (cyan). **(D)** Create a "Collection module" in Imaris, which will group all surfaces and spots from each N=10 cells rendered from the raw image together into one complete file. Next open collection as a Vantage Plot module within Imaris. Design a graph to plot GMFγ spots contacting zyxin and vinculin surfaces. Vantage Plot displays 5 separate GMFγ populations based on their proximity to vinculin and zyxin. **(E)** Imaris statistics can be extracted from the vantage plot and percentages of the total population outside and inside focal adhesions can be graphed. In addition, further analysis can determine the percent of GMFγ contacting vinculin only, GMFγ contacting vinculin in a focal adhesion containing zyxin, GMFγ contacting both vinculin and zyxin, and GMFγ contacting zyxin only.

AJRCMB Articles in Press. Published on 27-February-2019 as 10.1165/rcmb.2018-0352OC

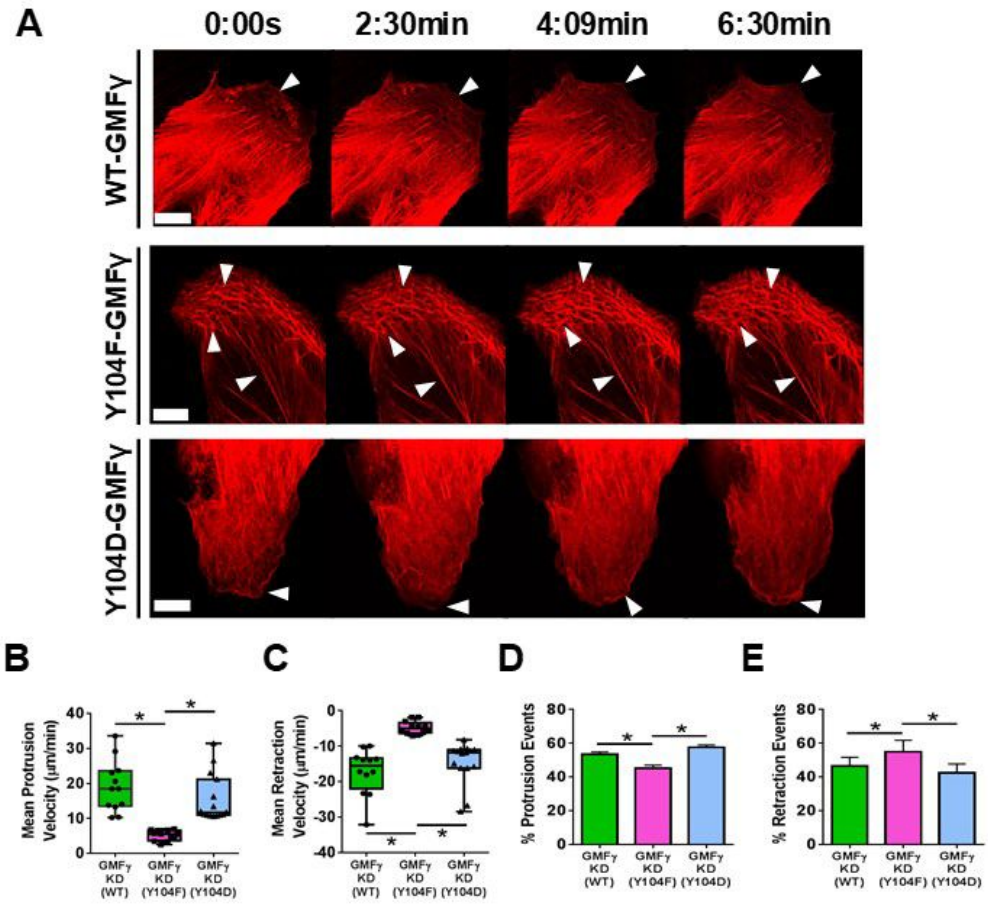

Figure S6: GMFγ phosphorylation at Y104 modulates lamellipodial dynamics. **(A)** GMFγ knockdown cells expressing WT, Y104F, or Y104D-GMFγ were transfected with LifeAct-RFP to monitor changes in lamellipodial dynamics. Live-cell imaging was performed on Zeiss LSM880 confocal with Fast Airyscan module. Images were taken every 10 seconds for a duration of 10 minutes, white scale bar = 10um. Arrowheads point to actin fibers and leading edge. **(B-E)** To quantify protrusion retraction dynamics we utilized the ADAPT ImageJ plugin (Methods, Barry 2015). The mean protrusion and retraction velocity, as well as percent protrusion and retraction events (WT = 5153, Y104F = 5990, Y104D = 4460), were calculated using the ADAPT plugin from 12 individual cells per expression plasmid. A one-way ANOVA with a Tukey's post hoc test to compare between groups was utilized for statistical analysis, p-value significance was *$p<0.05$.

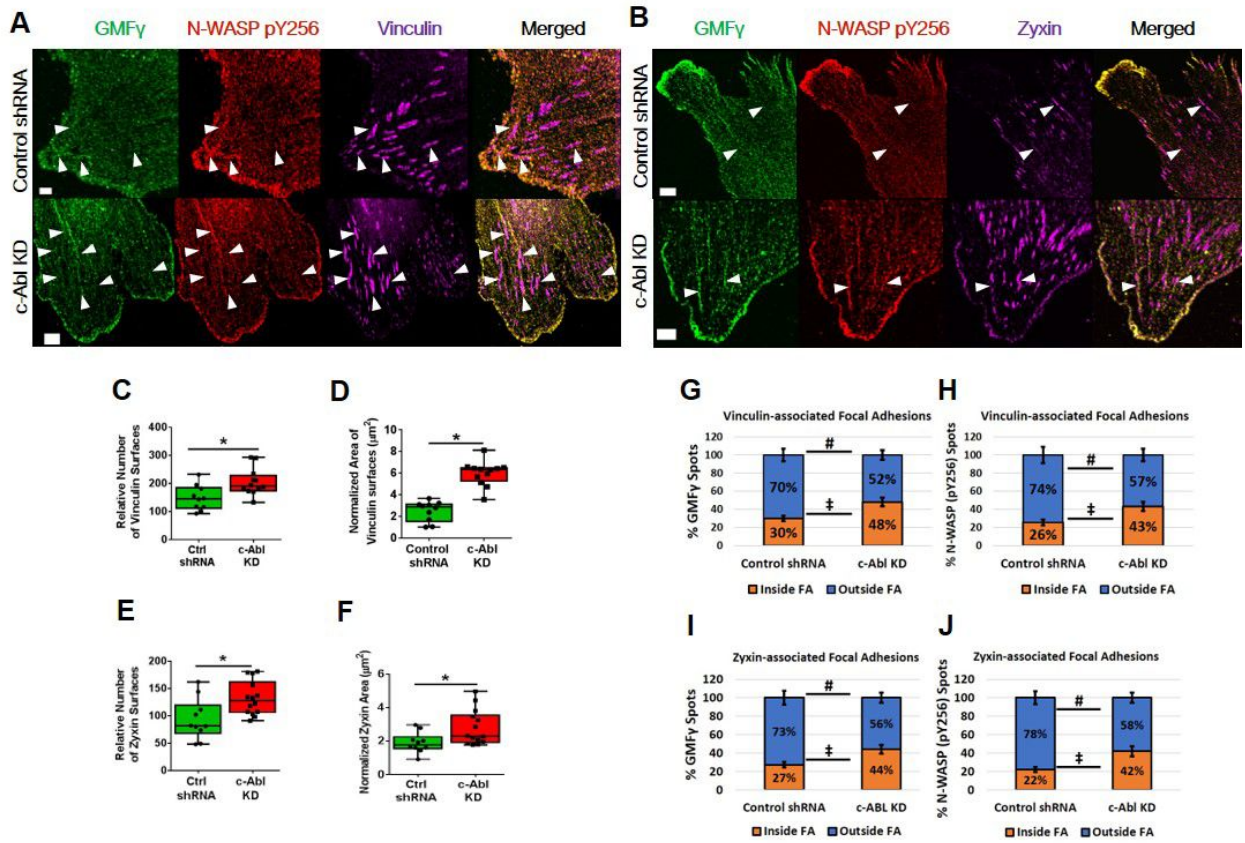

Figure S7: c-Abl knockdown increases GMFγ and N-WASP (pY256) recruitment to vinculin and zyxin-associated focal adhesions. (A,B) Immunofluorescent z-slice image taken using Fast Airyscan module on a Zeiss LSM880 confocal microscope. Arrowheads point to focal adhesions. **(C-F)** Input image into Imaris software. Utilize surface module to 3D-reconstruct vinculin (Control shRNA n=1,474, c-Abl KD n=2,250) and zyxin (Control shRNA n=933, c-Abl KD n=1,844) from n=10 individual cells into surfaces based on fluorescent intensity, area, and quality. Use Imaris statistics to acquire relative number per cell and surface area of vinculin and zyxin surfaces as previously described in Supplementary Figure 2. **(G-J)** Utilize spot module to 3D-reconstruct punctate GMFγ (n=23,210) and N-WASP (pY256) (n=27,084) into spots based on fluorescent intensity, number of voxels, and quality. Utilize MatLab "Spot to Surface" distance transformation algorithm to acquire percent GMFγ and N-WASP (pY256) inside or outside of vinculin or zyxin-associated focal adhesions. Statistical Analysis Student's T-test with significance indicated by *p<0.05, #p<0.05 for outside FA, ‡p<0.05 for inside FA from n=10 individual cells per treatment.

AJRCMB Articles in Press. Published on 27-February-2019 as 10.1165/rcmb.2018-0352OC

Movie 1: Phosphorylation state of GMFγ regulates human airway smooth muscle migration. Knockdown of GMFγ and expression of the non-phosphorylated Y104F-GMFγ decreased human airway smooth muscle migration, whereas expression of both the wild-type and phospho-mimetic Y104D-GMFγ enhanced migration.

Movie 2: GMFγ phosphorylation at Y104 impacts focal adhesion turnover and size. Non-phosphorylated Y104F-GMFγ enhances focal adhesion size, while decreasing focal adhesion turnover. Expression of phospho-mimetic Y104D-GMFγ decreased focal adhesion size and enhanced its turnover.

Movie 3: GMFγ phosphorylation at Y104 modulates lamellipodial dynamics. Non-phosphorylated Y104F-GMFγ decreased lamellipodial dynamics, while the expression of both wild-type and phosphorylated Y104D-GMFγ promoted lamellipodial dynamics.